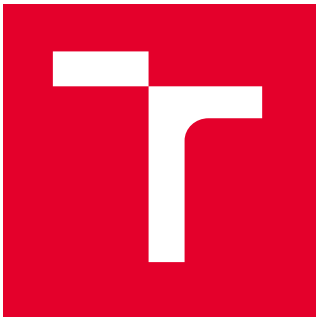

BRNO UNIVERSITY OF TECHNOLOGY

VYSOKÉ UČENÍ TECHNICKÉ V BRNĚ

FACULTY OF CHEMISTRY

FAKULTA CHEMICKÁ

INSTITUTE OF PHYSICAL AND APPLIED CHEMISTRY

ÚSTAV FYZIKÁLNÍ A SPOTŘEBNÍ CHEMIE

SEMICONDUCTOR MICROSTRUCTURES FOR CELLULAR PHOTOSTIMULATION

POLOVODIČOVÉ MIKROSTRUKTURY PRO FOTOSTIMULACI BUNĚK

MASTER'S THESIS

DIPLOMOVÁ PRÁCE

AUTHOR — **Bc. Anna Tvrdoňová**

AUTOR PRÁCE

SUPERVISOR — **doc. Eric Daniel Glowacki, Ph.D.**

VEDOUCÍ PRÁCE

BRNO 2023

BRNO UNIVERSITY OF TECHNOLOGY
FACULTY OF CHEMISTRY

Assignment Master's Thesis

Project no.:	FCH-DIP1836/2022	Academic year: 2022/23
Department:	Institute of Physical and Applied Chemistry	
Student:	**Bc. Anna Tvrdoňová**	
Study programme:	Chemistry and Chemical Technologies	
Field of study:	no specialisation	
Head of thesis:	**doc. Eric Daniel Glowacki, Ph.D.**	

Title of Master's Thesis:

Semiconductor microstructures for cellular photostimulation

Master's Thesis:

1. Perform a detailed literature survey of the use of semiconductor nano/microstructures for transducing optical signals to cells. 2. Use microfabrication techniques to create thin (<100 nm) metal/PN junction devices. 3. Pattern the metal/PN devices to have lateral dimensions in the range of micrometers, and functionalize them to have colloidal stability in physiological environment. 4. Use optical and electron microscopy techniques to image the resultant particles 5. Test the photocatalytic behavior with respect to oxygen reduction in physiological solutions 6. Plan cell experiments involving either controlled reactive oxygen species delivery and/or photocapacitive stimulation.

Deadline for Master's Thesis delivery: 8.5.2023:

Master's Thesis should be submitted to the institute's secretariat in a number of copies as set by the dean This specification is part of Master's Thesis

Bc. Anna Tvrdoňová student	doc. Eric Daniel Glowacki, Ph.D. Head of thesis	prof. Ing. Miloslav Pekař, CSc. Head of department

In Brno dated 1.2.2023

prof. Ing. Michal Veselý, CSc.
Dean

ABSTRACT

Hydrogen peroxide (H_2O_2) is a metastable reactive oxygen species regulating many biological pathways. The role of H_2O_2 in biological processes depends on its local concentration, in the nM range H_2O_2 can act as a signalling molecule, while exposure to higher levels of H_2O_2 can have cytotoxic effects. The aim of this work is to create photosensitive microparticles that would produce physiological amounts of hydrogen peroxide to regulate signalling pathways in cultured cells. The proposed microparticles are substrate-free organic photovoltaic elements that produce H_2O_2 by photofaradaic reduction of molecular oxygen with the concurrent oxidation of an electron donor present in the electrolyte. The detailed fabrication methods to achieve them were described. The particles have lateral dimensions in the range of micrometres, while a thickness of less than 100 nm. Photofaradaic reactions are driven by tissue-penetrating deep red light (660 nm) to enable potential *in vivo* applications of the technology. The thesis will discuss optimization of the photofaradaic microparticles production and characterization of the H_2O_2 evolution.

KEYWORDS

Electrostimulation, Photostimulation, Reactive oxygen species, PN junction

ABSTRAKT

Peroxid vodíku (H_2O_2) je metastabilní reaktivní forma kyslíku, která reguluje mnoho biologických drah. Úloha H_2O_2 v biologických procesech závisí na jeho lokální koncentraci, v malém množství (nM) může působit jako signální molekula, zatímco vyšší koncentrace mohou mít cytotoxické účinky. Cílem této práce bylo vytvoření fotosenzitivních mikročástic, které by produkovaly fyziologické množství peroxidu vodíku pro regulaci signálních drah v kultivovaných buňkách. Navrhované mikročástice jsou organické fotovoltaické struktury bez substrátu, které produkují H_2O_2 fotofaradickou redukcí molekulárního kyslíku. Produkce peroxidu probíhá za současné oxidace donoru elektronů přítomného v elektrolytu. Částice mají rozměry v řádu mikrometrů, zatímco jejich tloušťka nepřekračuje 100 nm. Fotofaradické reakce jsou poháněny červeným světlem (660 nm), které může pronikat tkáněmi, což umožňuje potenciální aplikace mikročástic *in vivo*. Práce se bude zabývat optimalizací výroby mikročástic a charakterizací produkce H_2O_2.

KLÍČOVA SLOVA

Elektrická stimulace, Fotostimulace, Reaktivní formy kyslíku, PN přechod

TVRDOŇOVÁ, Anna. Polovodičové mikrostruktury pro fotostimulaci buněk. Brno, 2023. Dostupné také z: https://www.vut.cz/studenti/zav-prace/detail/146802. Diplomová práce. Vysoké učení technické v Brně, Fakulta chemická, Ústav fyzikální a spotřební chemie. Vedoucí práce Eric Daniel Glowacki.

DECLARATION

I declare that the diploma thesis has been worked out by myself and that all the quotations from the used literary sources are accurate and complete. The content of the diploma thesis is the property of CEITEC and the Faculty of Chemistry of Brno University of Technology, and all commercial users are allowed only if approved by both institutions, the supervisor, and the dean of the Faculty of Chemistry, BUT.

……
student's signature

ACKNOWLEDGEMENT

I would like to express my sincere gratitude to my supervisor Eric D. Głowacki for giving me the opportunity to start an interesting journey of exploring the field of bioelectronics. Eric D. Głowacki has provided me with invaluable insights and suggestions that have helped me to shape my research and development. Eric, thank you for being optimistic and for always making time to discuss results and new ideas.

I would also like to thank my co-supervisor Marie Jakešová, who taught me everything in the cleanroom. I am grateful for her guidance, patience, and dedication to helping me achieve my academic goals. Maru, thank you for being my scientific mum and always being here for me.

Additionally, I would like to express my gratitude to my co-supervisor Jiří Ehlich, who designed and manufactured all necessary equipment for measuring. Jirko, thank you for your time, effort, and support.

However, nothing would be possible without my dear family and friends. Thank you for your love, support, and patience during my studies.

TABLE OF CONTENTS

1 INTRODUCTION

Bioelectronics is a field that merges the principles of biology, electronics, and engineering. It aims to create electric devices for biomedical applications. Implantable bioelectronic devices are designed to be placed inside the body. Therefore, there is an increasing demand in creating more minimalistic device architectures that decrease the physical and psychological load of implantation on patients. One strategy to producing less invasive devices is the use of wireless power transfer. Transduction of light into electrical power is the concept exploited in this thesis. The main objectives are based on an organic electrolytic photocapacitor device (OEPC or photocapacitos for short) that is generally used to convert short impulses of light into stimulating currents inside of tissue [1].

Photocapacitors contain two electrodes, a bottom return electrode with a photoelectrode on top. Generally, a substrate covered with conductive material serves as the return electrode, while an organic semiconducting material stack acts as the photoelectrode (Figure 1). The device was originally developed to operate in a capacitive manner, in which capacitive current should occur only at the start of the light pulse. The photogenerated charges are collected at the device – tissue interface creating two sets of charged double-layers. The discharging of the device occurs after the end of the light pulse and is exhibited as a capacitive current peak of opposite polarity. Such photocapacitors have been used to directly stimulate single cells, explanted retinal tissue, and *in vivo* peripheral nerves by acting on voltage-gated ion channels [1]–[4]. Besides that, the return electrode and the photoelectrode can support faradaic reactions as well. In such case, the capacitive charging is then followed by non-zero photocurrent during the rest of the light pulse. The capacitive vs. faradaic nature of the device can be tuned by choice of the materials [5].

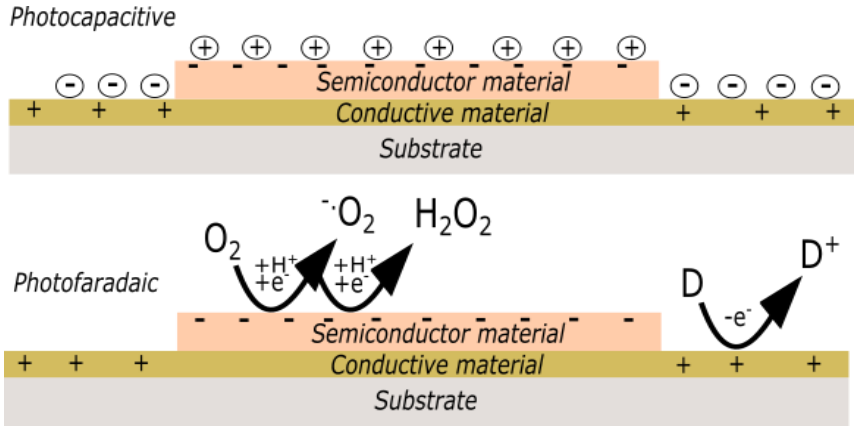

Figure 1 *Comparison of a photocapacitive and photofaradaic response after the absorption of light.*

Recent work of Gryszel and Głowacki reported the organic thin-film pixels utilized in physiological environment [6]. The device was designed and optimized to facilitate the photofaradaic mechanism. The efficient transduction of light into electrical power is then utilized to run redox reactions. Oxygen reduction reaction was the main focus of the work since it results in the generation of reactive oxygen species that can act as signalling molecules in the neural tissue [7]. The thesis drew inspiration from this work and aimed at producing a more efficient and facile alternative for *in vitro* and *in vivo* applications.

2 STATE OF THE ART

Stimulation of nerve tissue brought much attention to biomedical research in recent years. It is utilized in various neurotherapeutics and clinical applications [8], [9]. Materials such as semiconductors and metals are used to build devices that can be used for stimulation and recording of neural activity [10], [11]. However, one of the weak points of such devices is their electrical wiring and the necessity of an implantable power source, which complicates the surgery and increases the requirement for space. Photovoltaic stimulation represents an alternative technique where light is used as a wireless energy source, thus making it less invasive than conventional electrical stimulation [12].

Generally, biological tissue or even whole organisms can be stimulated by light [13]. The most known method for controlling cellular activity with light is optogenetics. The method genetically modifies target cells with light-sensitive proteins, enabling stimulation or silencing of different cell types [14]. Other approaches use photosensitive materials present in the near environment or directly within the cell. These materials act as light converters to other types of energy. The stimulation mechanism can be photothermal, photochemical, photofaradaic, photocapacitive, or a combination thereof.

Photothermal stimulation is caused by localized heating near the cell. The heat triggers an action potential via the stimulation of temperature-sensitive ion channels. This mechanism is strongly dependent on light intensity. The higher is the intensity, the faster is the temperature change [15], [16].

Photochemical stimulation changes the chemical environment around the cell. The reaction products can interact with various ion channels and lead to activation or silencing. The redox reactions occur on a single molecule or particle and must be balanced [5], [17].

Light conversion into electrical power is achieved by photocapacitive or photofaradaic mechanisms. In general, the devices used for stimulation are macroscopic. They consist of an insulating substrate, conductor, and semiconducting materials. In a photocapactive mode, the photogenerated charges separate, forming electrical double-layers of opposite polarities [5]. The spatial separation of charged surfaces affects the surrounding medium and generates capacitive current, which can trigger voltage-gated ion channels [18]. In a photofaradaic mode, the generation of current is accompanied by electrochemical reactions, the products of which can alter the electrophysiology as well. Often, the dominant cathodic reaction is reduction of oxygen to some form of reactive oxygen species [19].

2.1 Organic photovoltaic cells

Photovoltaic cells are semiconductor devices with the ability to convert light into electrical energy. Organic semiconductors are widely explored in the photovoltaic community due to their low-cost production and mechanical flexibility. Organics are especially useful in the context of this thesis where the generated electrical energy is further converted into chemical energy in the form of hydrogen peroxide. Many organic semiconductors reduce oxygen selectively to hydrogen peroxide [20].

Most conventional photovoltaics are made of inorganic semiconductors like silicon or gallium arsenide. These materials can absorb light and convert it into electrical power in a more efficient way in comparison to organic materials. However, they are not that flexible, thin, and easily tunable.

Organic semiconductor materials have a delocalized π-electron system that allows the transport of photogenerated carriers. There are two classes of organic semiconductor materials: small molecular weight organic compounds and conjugated polymers. There are p-type (donor) and n-type (acceptor) molecules, which can be put together to form a p-n junction. The molecular structure of the semiconductor molecule defines its band gap and thus the energetics of organic semiconductors can be easily tuned in contrary to inorganic materials [21], [22].

Organic photovoltaics are fabricated in a multilayer geometry. Glass or plastic is used as a substrate. The substrate covered with a conductive material serves as the bottom electrode. Next is a layer of semiconductive material or a heterojunction of semiconductors [23]. The two most-applied architectures are bilayer heterojunction (mostly used with small molecules deposited by vacuum evaporation) and bulk heterojunction (typically processed from a solution of polymer blend) [24]. The semiconductor layer is covered with a top electrode.

The energy levels of the donor and the acceptor molecules dictate the maximum achievable photovoltage. The mechanism of photocurrent generation is illustrated in Figure 2. Firstly, a photon hits the surface of the active molecule, resulting in a bound electron-hole pair *i.e.* an exciton. Then, the exciton diffuses to the interface between the donor and acceptor materials. The exciton then separates into an electron and a hole due to the potential offset between the two materials. The electrodes then collect the charges, resulting in the generation of photocurrent. The photocurrent value relies on the efficiency of each step [25].

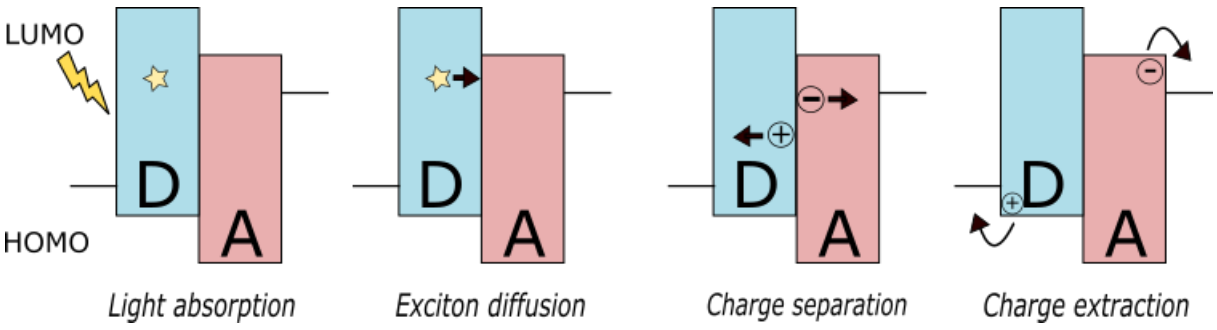

Figure 2 *Mechanism of photocurrent generation in an organic bilayer photovoltaic device.*

For example, phthalocyanine and perylene bisimide derivatives (Figure 3) are commonly found in thin-film organic solar cell applications [26], [27]. Phthalocyanine is a p-type material and acts as a donor. Phthalocyanines are commonly used as stable blue pigments. In contrast, perylene and its derivatives have n-type characteristics and are used as electron acceptors. They are widely used as red colorants with exceptional stability.

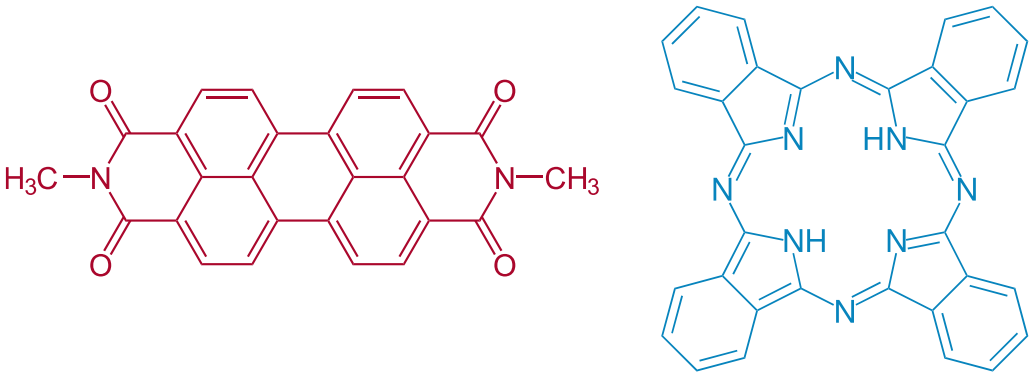

Figure 3 *Molecule of perylene bisimide (left) and phthalocyanine (right).*

2.1.1 Preparation

Vacuum evaporation and wet processing techniques are the most common for fabrication of organic solar cells. The material characteristics determine the choice of the process. Polymers are high molecular weight compounds that decompose at high temperatures. Therefore, wet processing at low temperatures is used to fabricate polymer-based photovoltaics. On the other hand, small molecules tend to be more stable and suitable for vacuum evaporation. [28].

Thermal evaporation is a relatively clean process. It is obtained under a vacuum of $< 10^{-5}$ mbar to reduce contaminants inside the chamber, like water and oxygen. These residues can be further reduced by using an ultra-high (less than 10^{-9} mbar) vacuum system or glove box with an inert atmosphere [24]. The evaporated molecule has a long mean free path and can travel directly without colliding with background gases.

Techniques used in wet processing are spin-coating [29], doctor blading [30], screen printing [31], and many others. Donor and acceptor blends are prepared by dissolving donor and acceptor components in a common solvent. The type of solvent depends on the donor-acceptor compounds.

2.1.2 Applications

Organic materials have lower power conversion efficiency than inorganic *e.g.* monocrystalline silicon solar cells. However, they will likely find more use in the future due to their tunable properties and possible adaptation into various related devices, as well as potential low-cost.

Organics are used in a wide range of applications, including displays, lighting, photovoltaics, sensors, and biotechnologies. Organic light-emitting diodes (OLEDs) are devices that emit light as a result of electric current flow. OLEDs are currently used in smartphones and televisions. Organic photovoltaics (OPV) do the opposite. OPVs transduce light to electrical current. Organic field-effect transistors (OFETs) are used as sensors within the applications

of environmental monitoring, and medical diagnostics. OFETs have high sensitivity, selectivity, and low power consumption. The property of some organic semiconductors to support both electric and ionic charge transport is used in biotechnology [32].

Organic semiconducting devices, as well as semiconducting particles [33], are being investigated for extracellular photostimulation of nerve tissue. Photocapacitors convert light into ionic current, which can result in stimulation of cell membrane [34]. This mechanism is considered photocapacitive. On the other hand, when exposed to light, devices and particles can also generate reactive oxygen species (ROS), which has attracted the attention of many studies [6], [35]. The generation of ROS, especially hydrogen peroxide, can be utilized to modulate living cells [36], [37]. Hydrogen peroxide (H_2O_2) is known as a toxic compound, however, in the lower concentration range, it can act as a signalling molecule [38]. H_2O_2 is generated by a two-electron oxygen reduction reaction and has been recently studied for various medical applications *e.g.* photostimulation of cells [39] or even cancer treatment [40].

2.2 Oxygen reduction reactions (ORRs)

The oxygen reduction reaction is based on single- or multi-electron transfer processes. An indirect two-step single-electron reduction leads to the production of hydrogen peroxide (Reaction 1 + Reaction 2). Moreover, peroxide can also be produced in a direct two-electron pathway (Reaction 3). The thermodynamics of each reaction can be characterized by the standard electrode potential E^0. Higher standard electrode potential reactions are more favorable thermodynamically. For a given reduction reaction to happen, the electrode potential has to be lower than its E^0 [41], [42].

$O_2 + e^- \rightarrow {}^{\bullet}O_2^-$ ($E^o = -0.35$ V vs NHE) ***Reaction 1***

${}^{\bullet}O_2^- + 2H^+ + e^- \rightarrow H_2O_2$ ($E^o = +1.46$ V vs NHE) ***Reaction 2***

$O_2 + 2H^+ + 2e^- \rightarrow H_2O_2$ ($E^o = +0.70$ V vs NHE) ***Reaction 3***

A four-electron oxygen reduction to water (Reaction 4) is thermodynamically more favorable than the two-electron pathway yielding hydrogen peroxide. However, these electrode potential values are considered under standard conditions, which would mean that all the species, H_2O_2 included, are at 1 M concentration. In the physiological environment, where the peroxide concentrations are much lower, the two- and four-electron pathways are thermodynamically more equal (around +1.2V). [43], [44].

$O_2 + 4H^+ + 4e^- \rightarrow 2H_2O$ ($E^o = +1.23$ V *vs* NHE) ***Reaction 4***

As this thesis is concerned with maximizing the production of hydrogen peroxide, it is important to consider the main pathway for loss of peroxide yield: the peroxide reduction reaction (Reaction 5). The two-electron reduction of peroxide results in water as a product and it is very favourable. However, considering kinetics of the reaction on the materials used within the thesis, the further peroxide reduction is not favoured until the peroxide concentration grows significantly.

$H_2O_2 + 2H^+ + 2e^- \rightarrow 2H_2O$ ($E^o = +1.76$ V *vs* NHE) ***Reaction 5***

2.2.1 Electrocatalysis

Electrocatalytic synthesis is an electrochemical process widely used in industry. An electrolyte solution and at least two electrodes with a catalyst are involved. The applied voltage forces a current flow, resulting in reactions on the catalyst. The main characteristics of an electrocatalyst are high activity, selectivity, and stability [45]. Reduction occurs on a cathode and oxidation occurs on an anode (Figure 4). Many researchers have achieved an electrochemical process with the selectivity of oxygen two-electron reduction to hydrogen peroxide [20], [46]–[48].

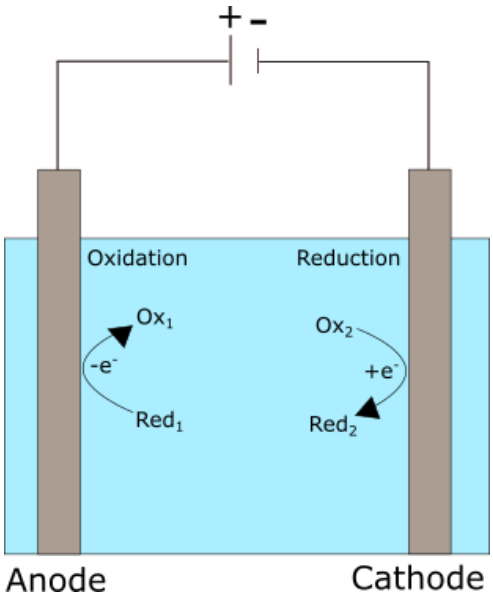

Figure 4 *Schematic process of electrocatalytic synthesis.*

2.2.2 Photo(electro)catalysis

There are ways in which photoelectrocatalysis and electrocatalysis are alike. The system consists of two electrodes (Figure 5). However, in photoelectrocatalysis, at least one of the electrodes contains a photocatalyst. The photocatalyst is a semiconducting material placed on the conductive substrate. The charge generation has the same principle as in photovoltaics. In comparison to photovoltaics, the top electrode is replaced by an electrolyte in the photoelectrode configuration. Therefore, the photogenerated charge carriers participate in redox reactions on the catalyst surface. There are two types of photoelectrodes. A photocathode uses the photogenerated electrons to reducuce some species in the electrolyte at its surface. A photoanode supports an oxidation reaction at its surface by the photogenerated holes [35].

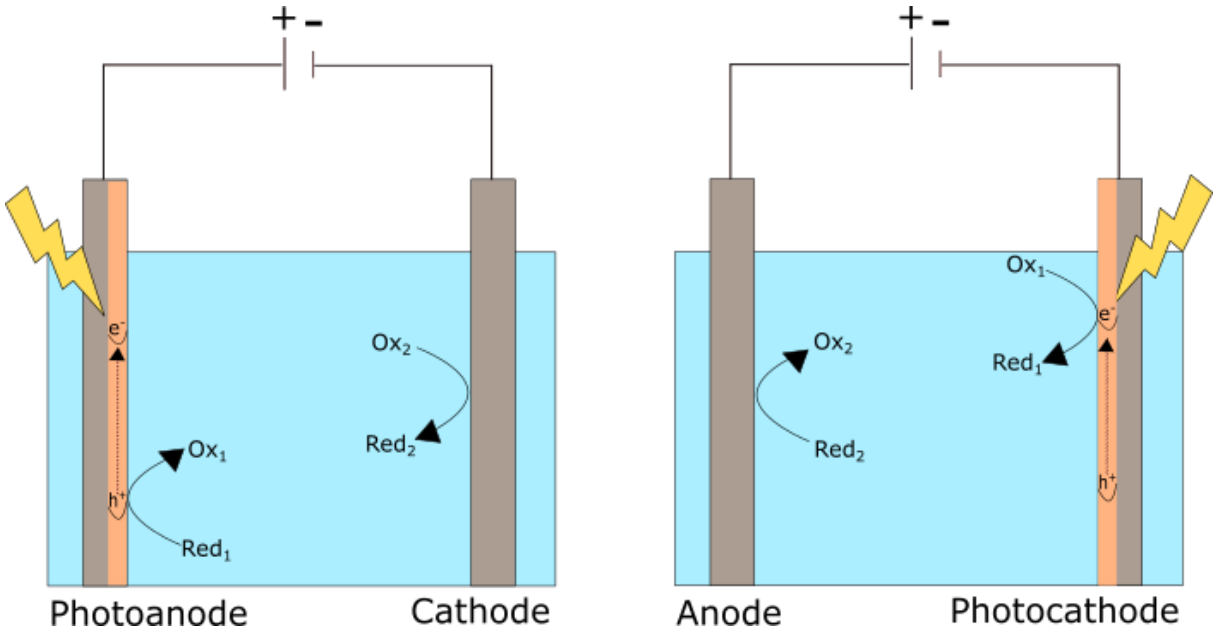

Figure 5 *Photoelectrocatalytic mechanism on a photoanode and a photocathode.*

2.2.3 Photocatalysis

Photocatalysis uses the same mechanism of charge generation as photoelectrocatalysis or photovoltaics. The system consists of a photocatalyst (semiconducting material) In contrast to photoelectrocatalysis, both reduction, and oxidation both take place on the particle surface (Figure 6). Photogenerated electrons and holes react directly with the species in the solution surrounding the photocatalyst [35].

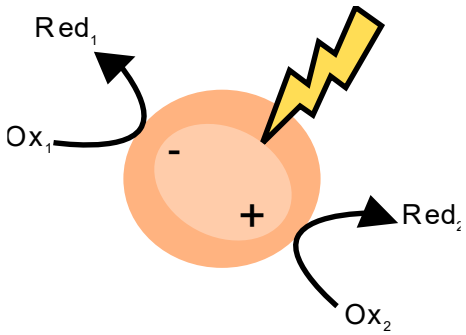

Figure 6 *Charge generation within the photocatalyst resulting in redox reactions.*

2.3 Cellular photostimulation

Cell membrane potential is characterized as the electrical potential difference across the membrane. The membrane utilizes ion pumps to actively regulate the levels of key ions like Na^+, K^+, Cl^-, and Ca^{2+}. Excitable cells, such as neurons and muscle cells can communicate via a sudden, fast, and propagating change in the membrane potential called the action potential (Figure 7). The resting potential of the membrane is negative. By applying an initial stimulus, the membrane potential depolarizes slightly and initiates the opening of voltage-gated sodium channels. The opening results in an influx of sodium ions into the cell, rapidly changing the membrane polarity. Once the membrane potential reaches positive values, sodium channels

inactivate and voltage-gated potassium channels open. The outward flux of potassium causes repolarization of the cell membrane. An active transport of ions by the sodium-potassium pump brings the system to the original equilibrium, the resting state [49].

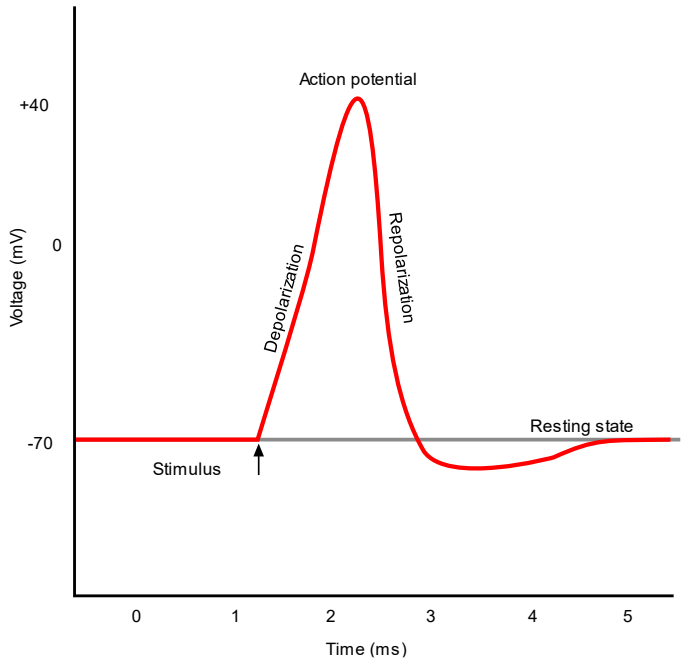

Figure 7 *Cell membrane voltage during an action potential.*

Electrostimulation is a widely used technique in electrotherapy that aims to provide the initial depolarization stimulus artificially. The system consists of wired electrodes, which are placed near the target tissue to be stimulated. By applying voltage, the electrodes generate current. The current flow causes a gradient of the membrane potential resulting in the generation of an action potential. With advanced technologies, the use of wiring is becoming less favorable. Thus, the interest in wireless stimulation techniques is increasing [50].

Additionally, recent works have demonstrated reactive oxygen species (ROS) as another alternative to stimulate cells [51], [52]. High levels of ROS lead to cell death. However, they can actively serve as important cellular messengers in a lower concentration range. Then, it is possible to trigger the action potential in certain cells by regulation of the peroxide levels. Each cell responds to ROS differently depending on its intra- or extracellular level. The most interesting candidate for stimulation by ROS is hydrogen peroxide [53].

3 AIM OF THE THESIS

The general aim of the thesis was to develop microstructures suitable for photostimulation of cells. The research covered the particle microfabrication and explored the photofaradaic mechanism of reactive oxygen species production. Optical and scanning electron microscopy were used to image the microstructures.

4 MATERIALS AND METHODS

4.1 List of chemicals

Chemical	CAS number	Brand
Acetone	67-64-1	Microchemicals
Ascorbic acid	50-81-7	BS Vinařské potřeby
Calcium chloride dihydrate	10043-52-4	Penta chemicals
Glucose	50-99-7	Carl Roth
Hellmanex	7778-53-2	Sigma Aldrich
HEPES	102571382	Sigma Aldrich
Hydrogen peroxide	7722-B4-1	Sigma Aldrich
Isopropyl alcohol	67-63-0	Microchemicals
Magnesium chloride hexahydrate	7791-18-6	Penta chemicals
Monopotassium phosphate	7778-77-0	Sigma Aldrich
Phosphate buffer saline	7647-14-5	Sigma Aldrich
n-octyltriethoxysilane	51851-37-7	Sigma Aldrich
Peroxidase from horseradish	9003-99-0	Sigma Aldrich
Poly(3,4-ethylene-dioxythiophene)	126213-51-2	Heraeus
Poly(4-styrenesulfonic acid) (6 % solution)	28210-41-5	Sigma Aldrich
Poly(vinyl)alcohol (M~31 000 g/mol)	9002-89-5	Microchemicals
Poly(vinyl)pyrrolidone (M~3 000 g/mol)	9003-39-8	Carl Roth
Poly(vinyl)pyrrolidone (M~360 000 g/mol)	9003-39-8	Carl Roth
Potassium chloride	7447-40-7	Penta chemicals
Potassium hydroxide	1310-58-3	Penta chemicals
Sodium chloride	7647-14-5	Lach-Ner
Sodium formate	141-53-7	Lachema
Sodium hydroxide	1310-73-2	Penta chemicals
Sodium phosphate dibasic heptahydrate	7782-85-6	Sigma Aldrich
Sulfuric acid	7664-93-9	Sigma Aldrich
3, 3', 5, 5'-Tetramethylbenzidine	54827-17-7	Sigma Aldrich

4.2 Fabrication

Most fabrication steps took place in the cleanroom of the Nanofabrication laboratory at CEITEC Nano, Brno University of Technology. Further characterization was done in general chemical laboratories.

4.2.1 Cleaning process

A cleanroom environment is beneficial during fabrication. The process starts with cleaning of the substrates (microscopic slides). Using an ultrasonic bath, the samples were sequentially cleaned in acetone, isopropanol, detergent solution (2 % hellmanex), and deionized water. The process is completed after the substrates are dried and stored in a box. Substrates are then placed into a Diener Nano Plasma Cleaner to activate the surface. The plasma cleaning process is performed in a vacuum chamber. Generally, oxygen and/or argon gas are utilized. Plasma removes all organic residues from the substrate, activates the surface by increasing the hydrophilicity, and improves adhesion [54]. Treatment with oxygen plasma was used within the thesis.

4.2.2 Spin-coating

Spin-coating is a widely used facile technique for fabricating thin films from solution. The liquid is placed in the centre of the substrate, which is then rapidly rotated (Figure 8). The final thickness is affected by the spinning speed, surface tension, and viscosity [55].

Various water-soluble polymer solutions of Poly(vinyl)pyrrolidone (PVP), Poly(vinyl)alcohol (PVA), and Polystyrene sulfonate (PSS) of different concentrations and molecular weights (Table 1) were spin-coated on the activated substrates. The process includes a slow spreading step (300 rpm, 5 s), and a second thickness-defining step (1500 rpm, 60 s). Right after, the samples were placed on a hot plate and heated for 10 min at 80 °C.

Table 1 *List of the polymer concentrations.*

Polymer	Concentration (%w/w)
PVP K90	2.0
PVP K12	2.0
PVP K12	10.0
PVP K12:K90 (7:2)	5.0
PVA	2.0
PVA	5.0
PSS	6.0

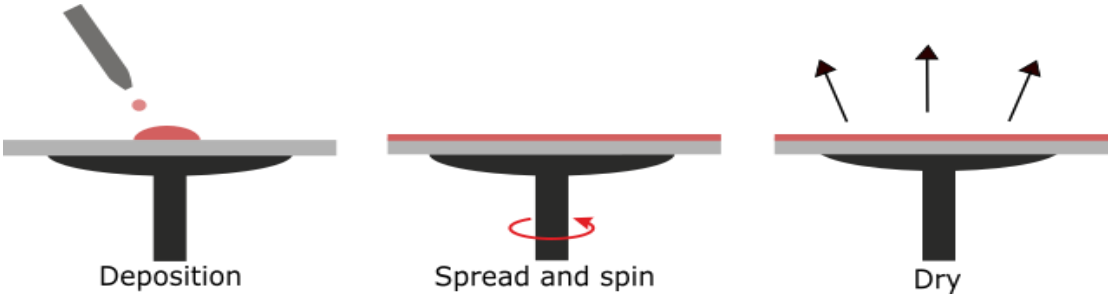

Figure 8 *Mechanism of the spin-coating method.*

4.2.3 Thin film deposition techniques

Physical vapor deposition (PVD) is a thin-layer technique allowing materials to transfer from a solid state to a vapor phase and condense on a substrate. Formation of the vapor phase is attained by resistive heating, electron-beam heating, or ion bombardment. Layer thickness is controlled by a quartz crystal microbalance (QCM) and a mechanical shutter under the substrate. To achieve layer uniformity, the substrate holder rotates during the deposition. PVD processes include evaporation and sputtering.

Evaporation is carried out in a vacuum environment. A high vacuum system prevents unwanted collisions with the vaporized material or contamination by residual gas molecules in the chamber. Source material can be placed into boats (typically metallic) or ceramic crucibles, depending on the material. The following text will describe the evaporation processes used in the thesis.

Electron beam (E-beam) evaporation uses an electron beam directed onto the target material, causing it to heat up and vaporize. Source materials are stored in pockets inside the chamber (Figure 9). This technique is commonly used for the evaporation of metals and oxides. In this work, a thin film of gold was deposited on the water-soluble layer. The deposition rate of gold (15 nm) was 1 Å/s.

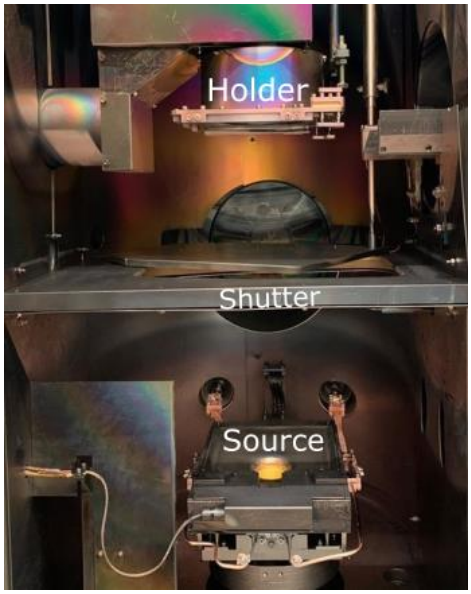

Figure 9 *Photo of components inside the E-beam evaporator chamber.*

Resistive thermal evaporation is the second PVD technique used. The source materials are in crucibles, that are enwrapped with tungsten wire and placed in a chamber (Figure 10). Then current is passed through the coil that causes resistive heating. The source is heated up, thus causing the evaporation of the material. It is followed by condensation onto the substrate in a uniform thin layer. The QCM monitors the deposition rate and determines the thickness. This method was used for the evaporation of the two organic materials. Phthalocyanine (H_2Pc) is a semiconducting pigment with high absorption coefficient. It is a p-type material and acts as a donor in our structure. The acceptor molecule was *N, N'*-dimethyl perylene tetracarboxylic diimide (PTCDI). The evaporation rates were ~3-6 Å/s for both materials, the deposition was done at a base pressure of $<1 \times 10^{-6}$ mTorr. Each layer was 30 nm thick. The combination of these two materials forms stable and effective organic PN heterojunction. Additionally, control samples containing solely the gold layer or the PN junction were fabricated.

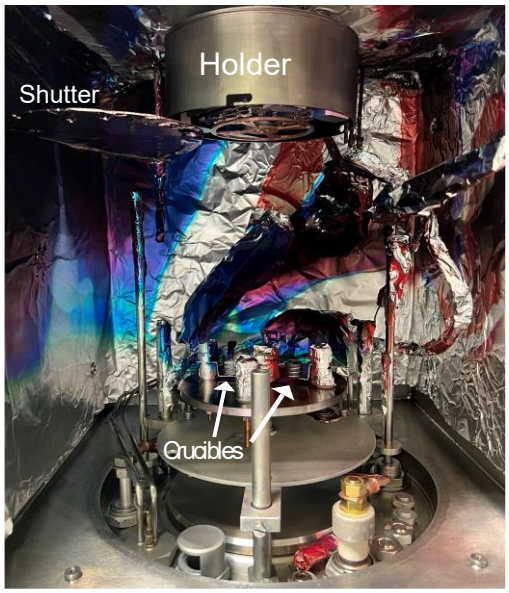

Figure 10 *Photo of the PVD chamber used for the deposition of organics.*

4.2.4 Free-floating system generation

The final sample contains multiple thin layers as shown in Figure 11. Due to polymer dissolution in an aqueous medium, the layer system can detach from the substrate. Only the polymer solutions that allowed facile detachment from the substrate were chosen for further fabrication. The samples were cut into 25 x 7 mm pieces for better handling and placed into *Eppendorf* tubes in pairs. The filler medium contained 0.1 % poly (vinyl)alcohol (PVA) solution. The polymer solution prevents particles from sticking to the surface of the tube. The samples were treated in ultrasound for 15 minutes to detach the film. Subsequently, the substrates were removed, and samples were sonicated for 5 minutes to further reduce the microparticle size. The final concentration of particles was 350 mm^2 per given volume (specified for each experiment).

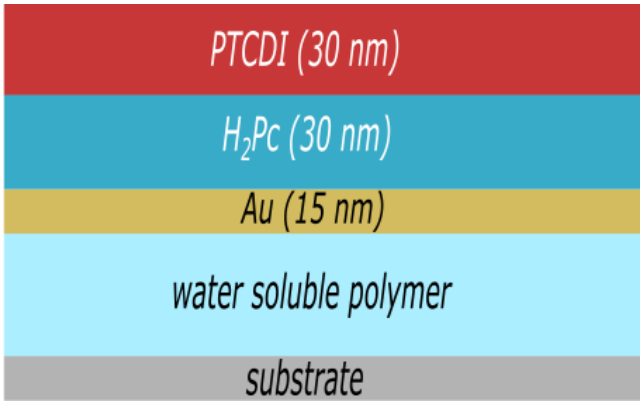

Figure 11 *Schematic of the fabricated multilayer on the substrate.*

4.2.5 2D planar devices

Planar devices (Figure 12) were fabricated to compare hydrogen peroxide production efficiency with the dispensed microstructures. Glass substrates were cleaned and treated with oxygen plasma for surface activation. Then, the substrates were covered with a mask during the evaporation to achieve an exact size of the active surface of the return electrode. A thin layer of chromium (1 nm at 0.3 Å/s) was evaporated to act as an adhesion layer for the gold electrode (9 nm at 1 Å/s). Following evaporation, the samples were placed into a chamber that contained vapor of n-octyltriethoxysilane (OTS) and held at 90 °C for 90 minutes. This treatment is crucial for the adhesion of organic layers and for preventing delamination [1]. After OTS treatment, the samples were sonicated in acetone for 5 minutes and rinsed with isopropyl alcohol, water, and dried. Next, a shadow mask was used during the deposition of organic layers under the base pressure of $<1 \times 10^{-6}$ mTorr and the deposition rates ~3-6 Å/s for both materials.

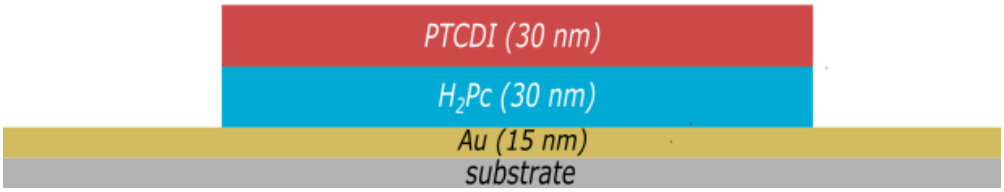

Figure 12 *Schematic picture of the planar device.*

4.3 Characterization

To compare photofaradaic and photocapacitive properties, the transient voltage generated by light pulses on the planar devices was measured. Next, the floating microparticles generated within the thesis were compared to the planar devices from the perspective of hydrogen peroxide production. Additionally, the particle system was characterized by two imaging techniques.

4.3.1 Transient voltage characteristic

The transient-voltage characteristic was measured to understand the device behaviour during light exposure (Figure 13). This type of measurement requires a rigid, planar structure that does not dissolve or detach from the substrate. The device was placed into a plastic Petri dish filled with phosphate buffer saline solution (PBS). The measurement uses an oscilloscope to measure the photovoltage transient. One of the electrodes is an Ag/AgCl wire enclosed in a syringe filled with PBS. The syringe opening was placed above the organic heterojunction (PN). The PN pixel was aligned in the centre of a red 660 nm light-emitting diode (LED). The second electrode was an Ag/AgCl wire that was dipped in the PBS far away from the device not to be affected by perturbations caused by the device, thereby serving as a reference electrode. The voltage transient in response to short light pulses was recorded. During the measurements, the positioning of the electrodes should be constant to obtain semi-quantitative data. The LED light intensity was 1.2 mW/mm^2. The characteristic was measured for planar devices made of glass, a gold return electrode, and a PN pixel in the middle of the device. One of the samples had islands of poly(3,4-ethylene-dioxythiophene) polystyrene sulfonate (PEDOT: PSS). The purpose of the PEDOT:PSS islands on the planar device is to act as a sacrificial electron donor.

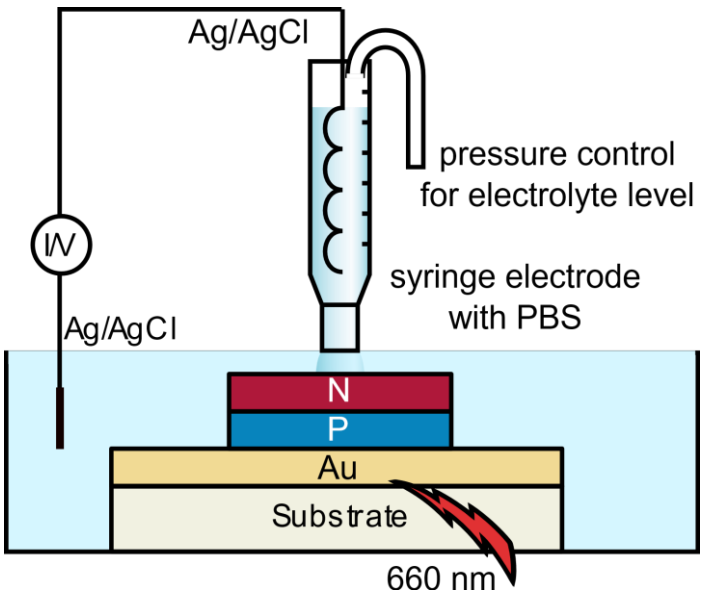

Figure 13 *The configuration for transient voltage measurement. Adapted from* [17] *with author's permission.*

4.3.2 Preparation of media

Following the fabrication of the microstructures, the donor solution was added in the form of glucose, sodium formate, or ascorbic acid. Considering the future application, more complex media were also used. In that case, the filler medium was removed after the detachment of microstructures and replaced with the complex one. The phosphate buffer solution (PBS) was chosen as a physiological-like solution. The artificial cerebrospinal fluid (ACSF) is more sophisticated. The filler solution of PVA was used as a standard. The composition of each medium is listed in Table 2.

Table 2 *Constituent components of the media.*

ACSF (Patch-clamp medium)		**PBS**		**Filler medium**	
Compound	*c* [mM]	Compound	*c* [mM]	Compound	*c* [mM]
NaCl	140.0	NaCl	8.0	PVA	0.03
$CaCl_2$	2.5	KCl	0.2	Donor	10.0
$MgCl_2$	2.0	Na_2HPO_4	1.4		
HEPES	10.0	KH_2PO_4	0.3		
Glucose	20.0				
KOH	3.0				
NaOH	2.0				

4.3.3 Light-mediated production of hydrogen peroxide (H_2O_2)

The measurement was done in a filler medium with addition of 10 mM donor concentration. The sample was placed above the light source, as shown in Figure 14. The illumination was provided using a 660 nm light-emitting diode with a light intensity of 50 mW/cm^2. The intensity was calibrated using a Thorlabs Si p-i-n diode (Thorlabs SM1PD1B). The final volume, particle concentration, and exposure time were set for each experiment separately.

Figure 14 *The illumination of the samples inside the holder on the LED array.*

4.3.4 Quantification of H_2O_2

Multiple methods can be used to quantify hydrogen peroxide, such as amperometric detection, fluorescent probes, or spectrophotometry assay used within the thesis. H_2O_2 is an oxidant, and the method is based on its reaction with a colour-forming oxidizable substrate. Colourless substrates get oxidized by hydrogen peroxide, resulting in coloured products. In our lab, we use tetramethylbenzidine (TMB) and measure the absorbance at 653 nm. The Horseradish peroxidase (HRP) enzyme catalyzes this reaction. The reaction is carried out in a buffer solution at pH 5.6 made of citric acid and Na_2HPO_4. For every measurement, a new assay mixture containing the buffer, HRP, and TMB was prepared and stored for a maximum of 5 hours at 10 °C.

Preparation of buffer solution

Solutions of 0.2 M Na_2HPO_4 and 0.1 M citric acid were mixed to obtain a buffer pH of 5.6.

Preparation of TMB and HRP stock solution

The TMB was dissolved in DMSO to yield a final concentration of 10 mg/mL. The HRP type I with an activity of 89.90 U/mg, was used to make a 2 mg/mL solution. Both solutions were divided into 1 mL aliquots and were stored at −20 °C.

Preparation of the mixture for analysis

The assay mixture contains 10 µL HRP and 25 µL of TMB in 4.96 mL of 0.1 M buffer. The ratio between the assay mixture and the H_2O_2 sample depends on the peroxide concentration since the final peroxide concentration should not exceed 40 µM. Throughout this study, we mixed it in a ratio of 5:2 (buffer: sample). Upon mixing,a blue product is formed. A plate reader was used to read the absorbance in 96-well plateswith a final volume of 100 or 200 µL. If the hydrogen peroxide concentration is higher than ~50 µM, the solution will turn green/ brown.

Preparation of the calibration curve

First, the exact concentration of a commercial 30 % H_2O_2 solution was determined by titration with standardized potassium permanganate. The titrant was a 0.2 M solution of potassium permanganate. The analyte contained 50 µL of H_2O_2, 2 ml 96 % H_2SO_4, and 20 ml of water. The measured concentration of the commercial H_2O_2 was 10.07 M.

Then the peroxide solution was diluted to a concentration of 100 µM and used for the construction of the calibration curve. The solution was mixed with the assay solution in final concentrations of 0.5, 2, 5, 10, 20, 30, and 40 µM. The measurements were done in two final volumes, 100 and 200 µL. The absorbance was measured at 653 nm (Figure 15).

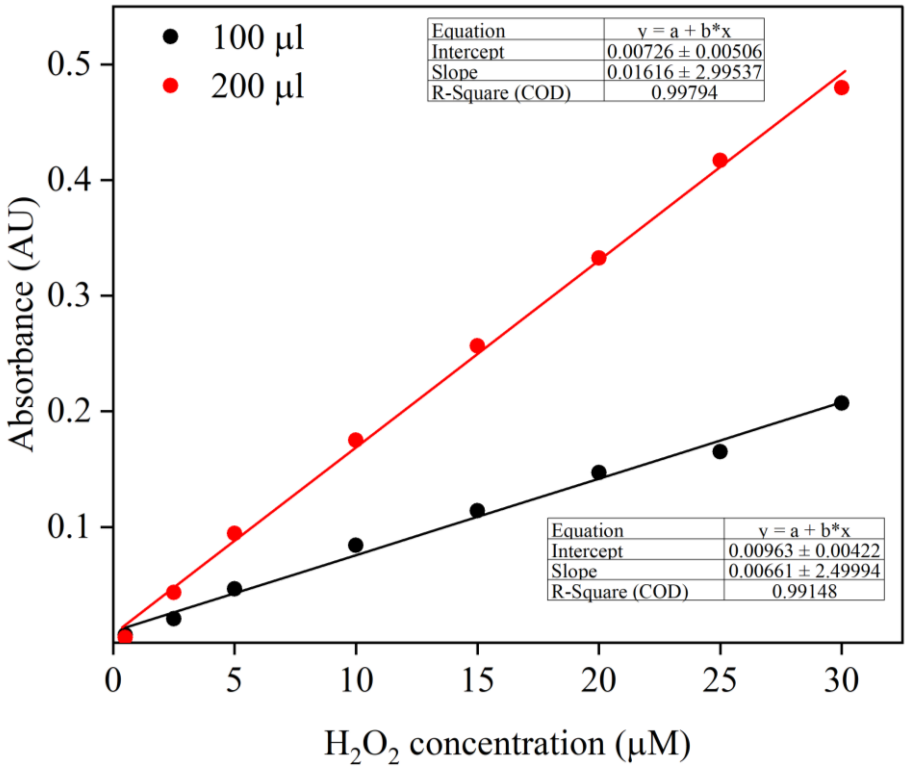

Figure 15 *H_2O_2 calibration curve for volumes of 100 and 200 µL.*

A linear regression equation (Table 3) was obtained from the calibration curve and used further to evaluate H_2O_2 concentration.

Table 3 *The coefficient (a), (b), and coefficient of determination (R^2) for each volume.*

Volume (µL)	a	b	R^2
100	0.0066	0.0096	0.9915
200	0.0162	0.0073	0.9979

4.3.5 SEM and optical microscope imaging

Optical microscopy uses visible light to visualize objects in the range of micrometers. It is one of the oldest and most widely used imaging techniques. The basic components of a microscope include a light source, a condenser lens, an objective lens, an eyepiece, and a camera. The light from the source goes through the condenser lens and directly on the substrate. The objective lens magnifies the image which the camera can take. The microparticles were deposited onto a silicon wafer and visualized.

Scanning electron microscopy is an imaging technique with several advantages over other forms of microscopy. For example, the ability to provide high-resolution images of the surface, with a resolution as high as 0.1 nm. The resolution is achieved by short wavelength of the electrons. The electrons coming from the beam interact with electrons of the atoms in the sample, emitting secondary electrons, backscattered electrons, and characteristic X-rays. Various detectors collect the signals, and the information is used to provide a detailed sample image. High-resolution Scanning Electron Microscope FEI Verios 460L was used for the purpose of the thesis. Using low acceleration voltages (< 3 kV) to image organic materials is necessary, because they are more sensitive to electron beam damage. Moreover, the image contrast is higher due to reduced sample charging.

5 RESULTS AND DISCUSSION

5.1 Transient-voltage characteristic

It is important to distinguish between the photofaradaic and the photocapacitive operation modes. The photocapacitor charges up at the beginning and discharges at the end of the light pulse. The mechanism uses pulses, which generate the current flow for the photocapacitive stimulation processes. Considering the photofaradaic mechanism, redox reactions must be present. Redox reactions occur on the device surface surrounded by a medium. Donor molecules are required within the medium or on the device structure to support oxidation reactions. Therefore, one of the devices had additional islands of PEDOT (Figure 16). The role of PEDOT is to act as a sacrificial donor molecule, which should help to improve the photofaradaic character. The transient-voltage (V_t) characteristic was examined (Figure 17).

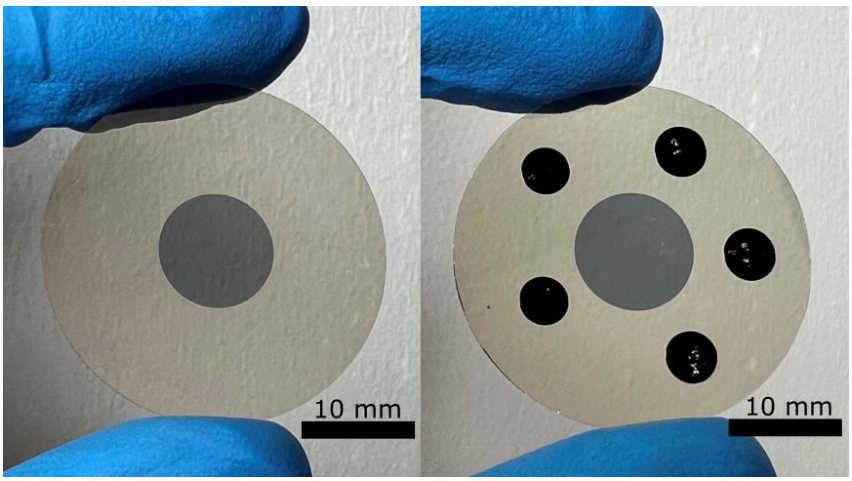

Figure 16 *Planar devices with gold layer and PN in the center (left) with PEDOT islands (right).*

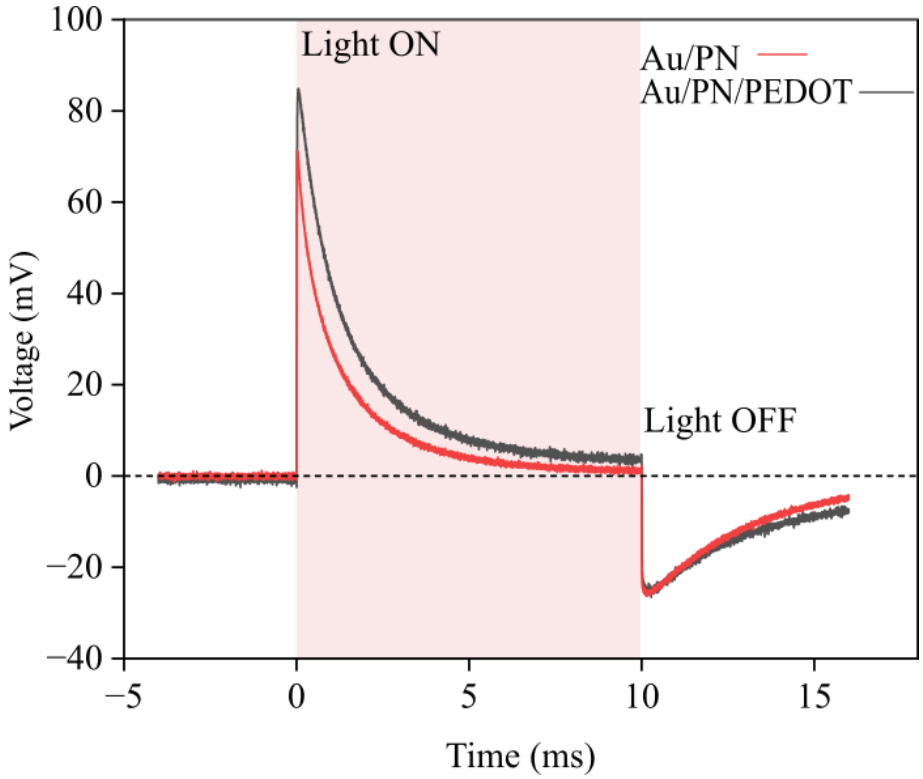

Figure 17 *Comparison of transient voltage characteristics for Au/PN device vs. Au/PN with islands of PEDOT.*

The device with Au/PN layers showed partial photofaradaic characteristics within the duration of the light pulse. The device charged up at the beginning, only after a few miliseconds the transient voltage value was approching zero, indicating that some faradaic current was flowing. The discharging peak occurred after the end of the light pulse. The sample with Au/PN and PEDOT islands charging peak was slightly higher and the transient stays non-zero within the duration of the light pulse. This sustained current indicates a faradaic redox pair. Considering that PEDOT:PSS acts as a sacrificial donor, an increase in faradaic behaviour was indeed expected.

5.2 Fabrication of microstructures

The choice of water-soluble polymer is crucial for the fabrication. It causes the layers to detach from the substrate in a water-based solution. The homogeneous polymer layer was made by spin-coating. The samples containing PVP K12 formed an uneven layer. The rest of the samples with PVP K90, PVA, and PSS produced uniform layers and were used for full device fabrication. The final samples (Figure 18) were investigated for detachment of Au/PN layers (Figure 19).

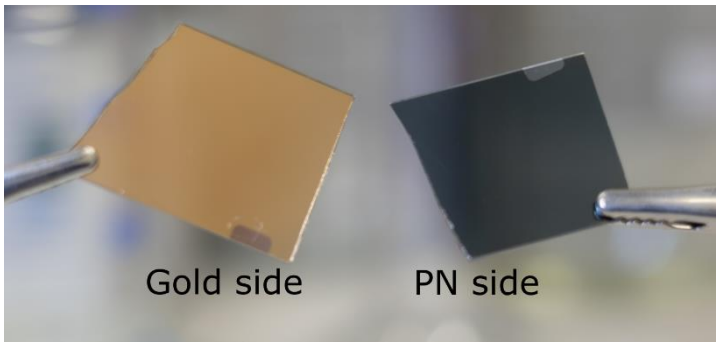

Figure 18 *The substrate from bottom (gold) and top (PN).*

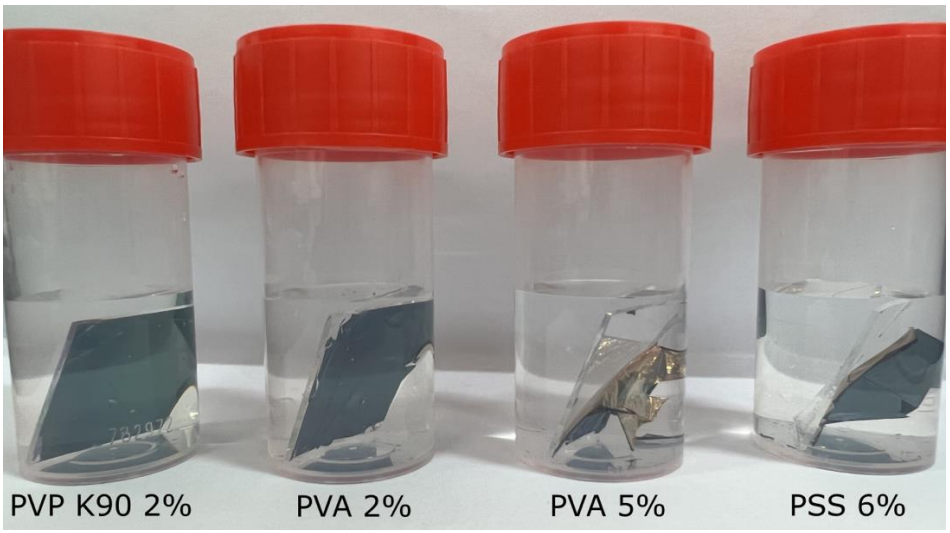

Figure 19 *The layer system detachment from the substrate after 4 hours in water.*

The sample containing the PSS polymer layer immediately detached slightly after contact with deionized water. The layer detachment was completed after 4 hours. The same was true for the sample with a 5 % PVA polymer layer. However, the samples with 2 % PVP or PVA did not detach at all. This phenomenon proved that the polymer concentration and composition affect the solubility and influence whether or not the layers detach from the substrate. Therefore, 5 % PVA or 6 % PSS were both suitable for fabrication. The solution of PSS is more acidic and did not prevent the microstructures from sticking to the surface of the tube. Therefore, the PVA was chosen as the standard polymer layer. The overall process of the final microstructure production is pictured in Figure 20.

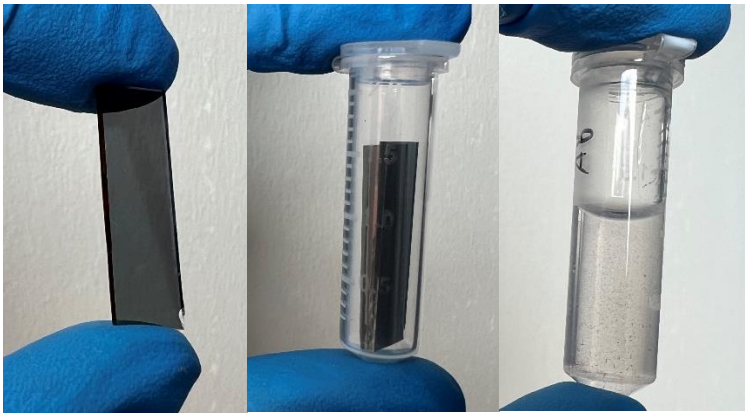

Figure 20 *The process of microstructure preparation in an Eppendorf tube, involving inserting the rigid substrate into the aqueous polymer solution and then using sonication to detach and break up the semiconductor device layers.*

5.3 Production of H_2O_2

The photofaradaic mechanism was preferred within this thesis. The particles dispersed in a medium containing electron donor were illuminated with red light. The photofaradaic production of H_2O_2 starts immediately after exposure to the light (Figure 21). Upon illumination, the n-layer is polarized negatively and catalyzes the oxygen reduction to hydrogen peroxide. Simultaneously, oxidation of the donor molecules on the surface of the positively polarized gold layer closes the redox cycle.

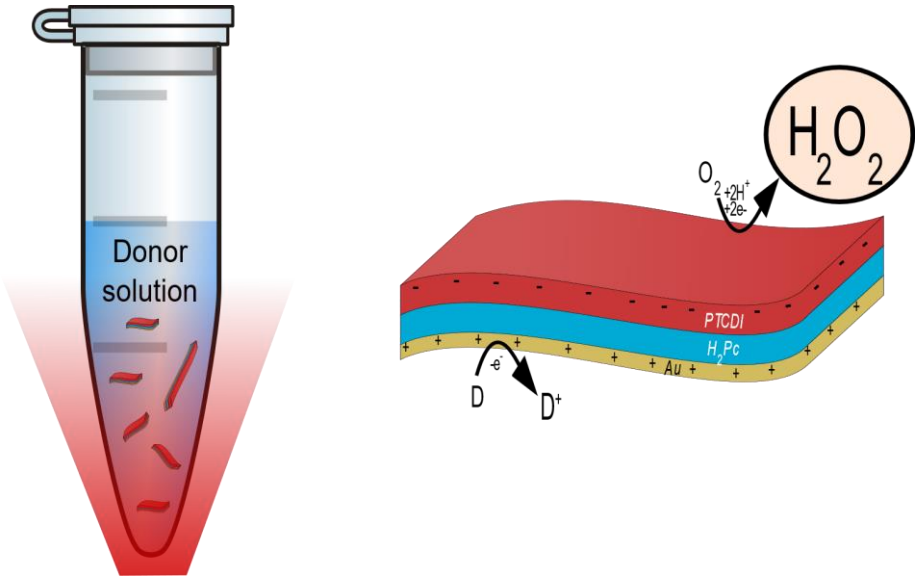

Figure 21 *Mechanism of exposure to the deep-red light resulting in redox reactions on the microparticle surface.*

The filler medium was used to understand the effect of different electron donors on the efficiency of H_2O_2 generation. The polymer in the filler medium prevents the particles from attaching to the *Eppendorf* tube walls. The donors investigated were glucose, ascorbic acid, and sodium formate at 10 mM concentration. The donor was added in excess. The production of H_2O_2 was quantified hourly with the spectrophotometric assay. The total exposure time was 3 hours, and the results are shown in Table 4.

Table 4 *Comparison of donor efficiency during photofaradaic evolution of H_2O_2.*

Time (h)	**H_2O_2 concentration (μM)**		
	Ascorbic acid	Glucose	Sodium formate
1	0	0	12
2	0	2	30
3	0	4	46

The samples containing ascorbic acid showed no presence of H_2O_2 even after 3 hours. Ascorbic acid is a strong antioxidant that acts as a reducing agent for free radicals. Therefore, we believe, that the evolved H_2O_2 is immediately reduced. The concentration reached a maximum of 4 μM when using glucose as a donor. Glucose is a good electron donor, however, the catalytic activity of the gold surface gets poisoned by the oxidation products [6]. The highest peroxide production was achieved with sodium formate. The molecule is oxidized to the form CO_2, which does not affect the gold surface. Based on the results, sodium formate was chosen as a donor for further experiments.

The ACSF and PBS were representative media to simulate physiological conditions. Since the ACSF contains a lot of promising compounds that can be oxidized, adding extra donor was not necessary. In case of PBS, the donor used was sodium formate. The filler medium containing PVA and sodium formate as the donor was used as standard. The total time of light exposure was 5 hours (Figure 22).

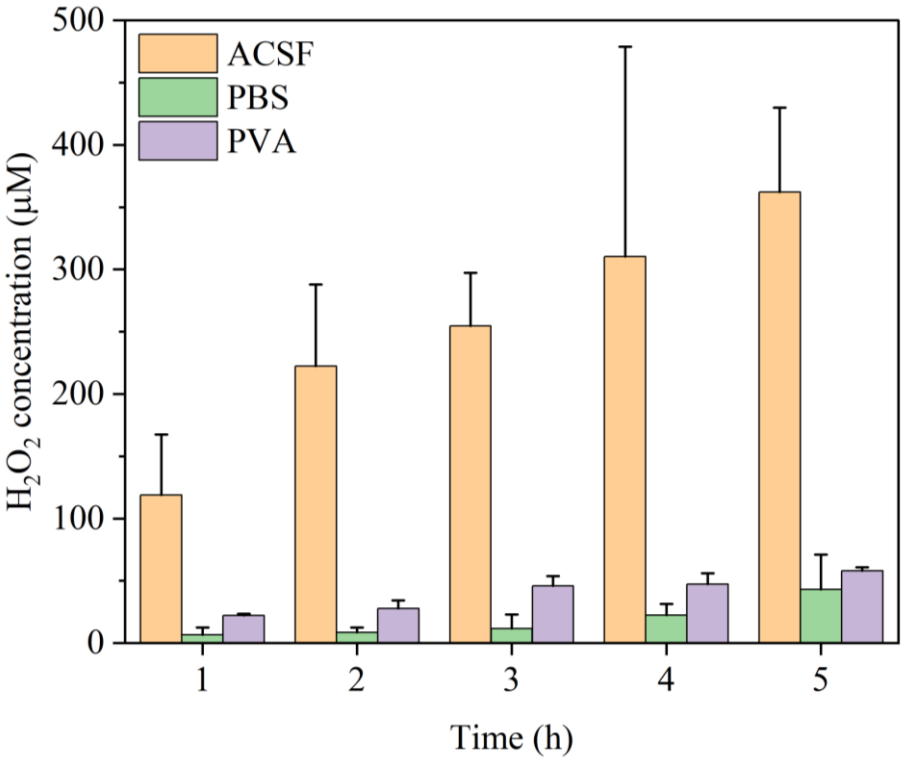

Figure 22 *Comparison of H_2O_2 production in different media. 750 μL, 350 mm² of particles*

Even though the presence of glucose in ACSF could lower the catalytic activity of gold, significantly higher H_2O_2 concentrations were achieved in this media. The concentration was over 100 μM after one hour of exposure to the light. It was confirmed that the efficiency increase was caused by HEPES being an excellent donor [56]. Since HEPES is not a physiological molecule, this result is only relevant for *in vitro* studies. The particles were more colloidally stable in ACSF, so it was impossible to separate the particles from solution by centrifuge completely. Presence of particles in the measured aliquots could result in higher variance of the samples. The yield in PBS solution was slightly lower than in the standard PVA filler solution. The PVA with sodium formate was chosen as a standard because the evolution of H_2O_2 is approximately the same for every measurement within the thesis.

5.4 Planar devices vs. microstructures

In order to benchmark the microstructures it was necessary to compare their efficiency with a (rigid) planar device of equivalent active areas. The active area of each the Au layer and the PN layer was ~79 mm² (Figure 23). A final volume of 1500 μL of the filler medium with sodium formate was used for both types of samples. The samples were placed above

the light source. Otherwise, the experiments were held under the same conditions for both planar devices and microparticles (Table 5).

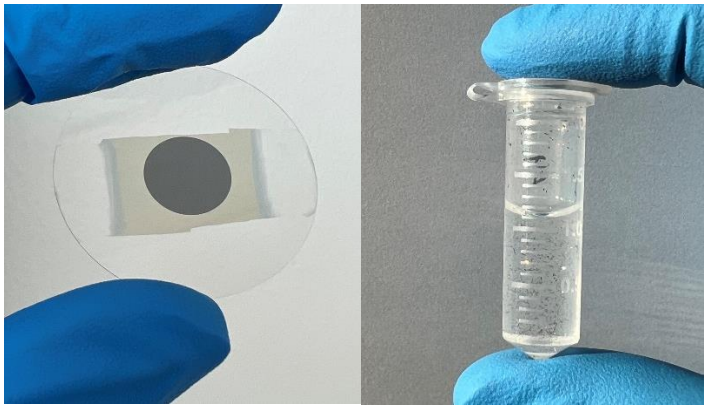

Figure 23 *Planar devices and microstructures used for efficiency comparison. In this case the area of active materiál was kept the same for both samples.*

Table 5 *Comparison in the H_2O_2 generation by planar devices and microparticles.*

	H_2O_2 concentration (μM)	
Time (h)	planar device	Microstructures
1	0	1.5
2	0.6	3.2
3	0	4.5
4	0	5.2
5	0	9.6

The 2D planar device showed basically no production of H_2O_2, because it occurs only in the vicinity of the surface / environment interface area. On the other hand, floating microstructures can produce H_2O_2 in whole volume, resulting in high efficiency. Within reason, the smaller the particles are, the more suitable for certain applications *e.g.* injection into the body.

5.5 Efficiency, reproducibility, and stability

Following the successful fabrication process, the behavior of the microstructures was examined under different conditions. Efficiency, reproducibility, and stability were the main characteristics studied within the thesis. First, the efficiency in the production of H_2O_2 was investigated for Au/PN microstructures. To prove that the whole stack is necessary for efficient photofaradaic peroxide production, microparticles made of bare layers of Au and PN were used as controls. The time of exposure to the light was 8 hours (Figure 24).

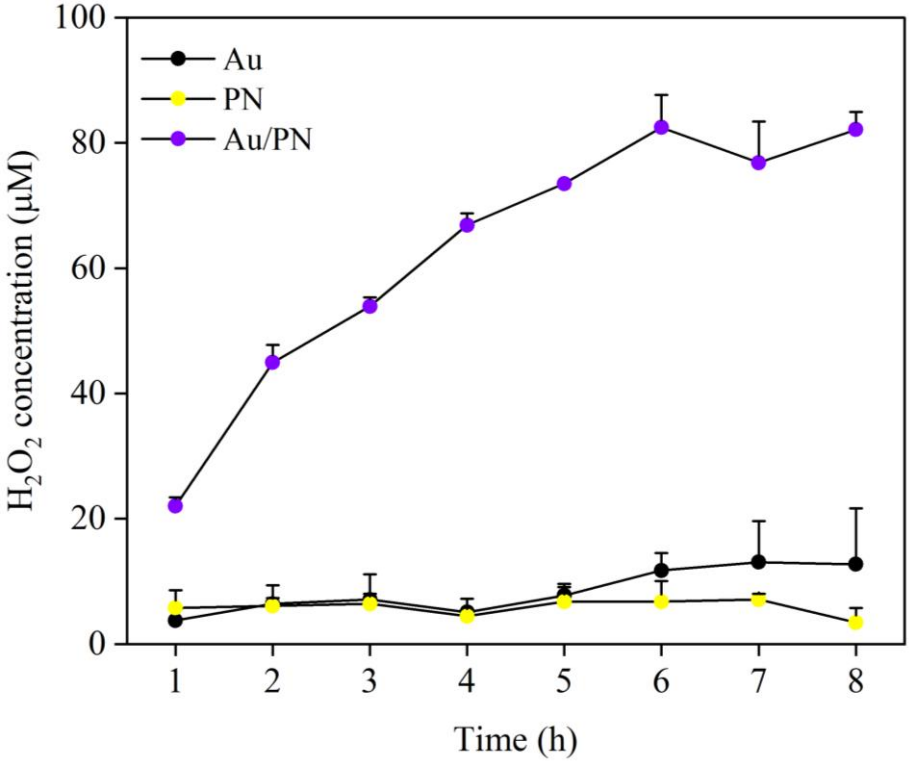

Figure 24 *Comparison of different H_2O_2 production mechanisms.*
Filler medium: 750 μL, 350 mm² of particles

The full stack devices (Au/PN) continuously produce peroxide as shown in the previous sections. The H_2O_2 concentration is saturating after about 5 h at 80 μM. The saturation can be caused by reaching high H_2O_2 concentrations within the medium. Then, the further H_2O_2 reduction to water can take place. Another reason could be limited catalytic activity of the gold layer, however, it is not decresing as fast as with glucose as the donor.

As expected, both the control samples produce significantly less peroxide, however, the levels are non-zero in both cases. The Au particles could generate H_2O_2 due to the presence of plasmonic effects [57]. While the PN particles could produce small amount of peroxide by photocatalysis via autooxidation mechanism [37], [58]. This process causes slow degradation of the material itself. The concentrations produced by the controls reached approximately 10 μM. These values were not changing significantly during the whole course of the measurement. These results indicate that the combined stack Au/PN particles work in a photofaradaic manner.

The concentration of particles in the studied sample will also influence the rate of H_2O_2 evolution. To investigate such behaviour, a 350 mm^2 of particles was dispersed in different volumes of the filling medium (Figure 25).

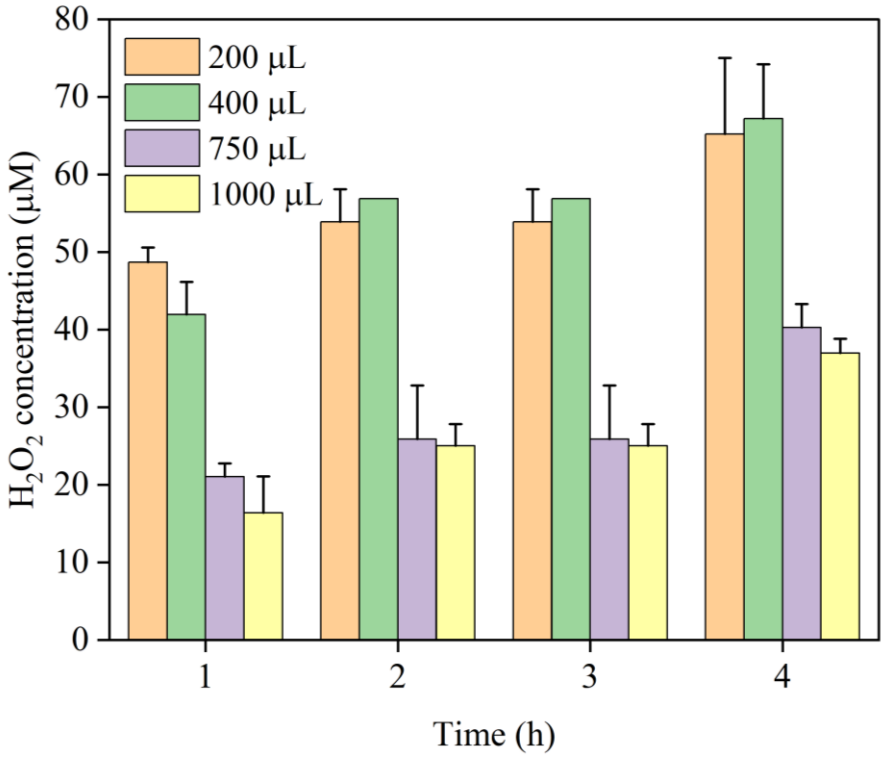

Figure 25 *Influence of the particle concentration on the H_2O_2 concentration produced. Filler medium: 200–1000 µl, 350 mm^2 of particles.*

Each sample contained the same total amount of particles. The higher the volume of the sample (the lower the particle concentration) the slower was the production of H_2O_2. High concentration of the particles resulted in a high speed of H_2O_2 evolution. However, the concentration is saturating after about 2 hours (Figure 26).The less concentrated particle solutions produced a steady increase in hydrogen peroxide concentration.

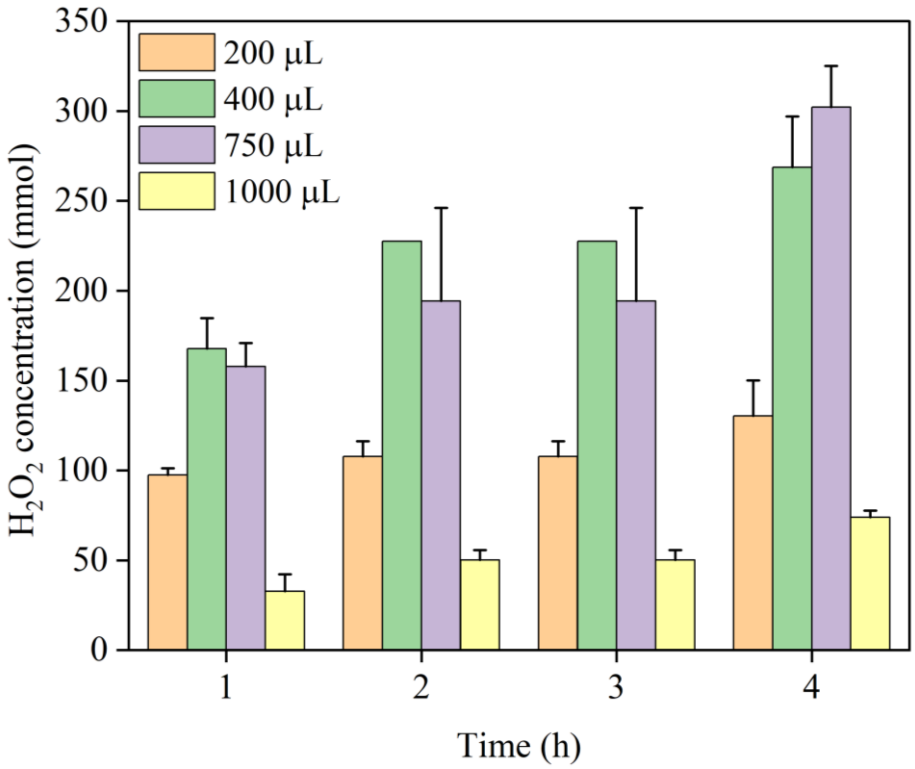

Figure 26 *Influence of the particle concentration on the H_2O_2 amount produced. Filler medium: 200–1000 µl, 350 mm² of particles*

To evaluate the reproducibility of the particle preparation, we compared samples from two different fabrication batches (Figure 27). The performance for Batch 1 and 2 was similar, and thus the process reproducibility was satisfactory. Another proof of reproducibility is that all graphs above (with the same particle concentration and volume) achieved the same peroxide evolution reaching around 50 µM in 3h.

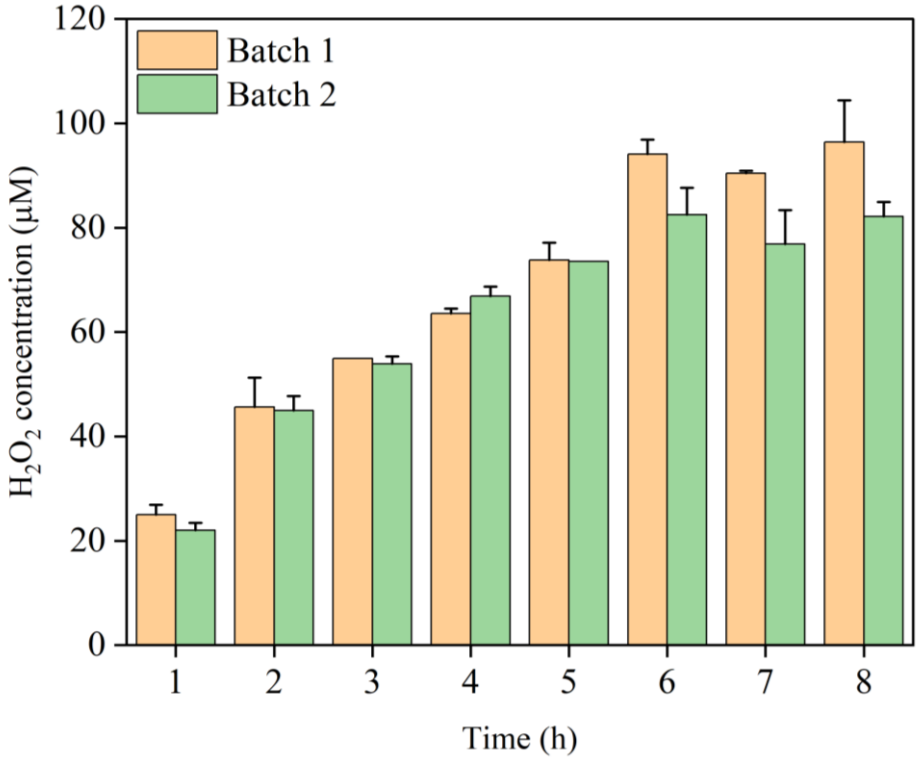

Figure 27 *Comparison of H_2O_2 production by two different fabrication batches. Filler medium: 750 μL, 350 mm² of particles*

Finally, we studied the functional stability of the particles during multiple runs of photofaradaic synthesis in fresh media. After each 1 hour illumination run, the particles were centrifuged, the used medium was collected, the particles were washed two times, and mixed with a fresh filler medium containing sodium formate. The peroxide concentration in the samples was measured after 15 and 60 minutes of illumination. The whole process was repeated 8 times (Figure 28). For the first three cycles, the production efficiency was increasing. During the next five cycles, the production steadily decreased. This could be explained by a few reasons: the catalytic activity of the gold layer was steadily decreasing; some particles were lost during the washing steps; the particles started aggregating due to the handling.

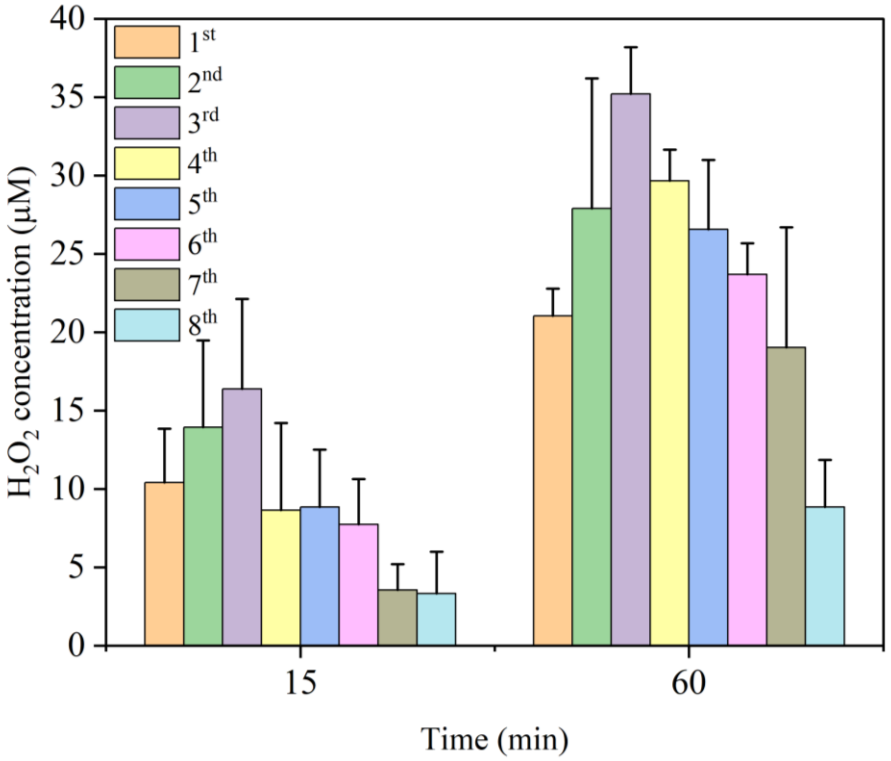

Figure 28 *Comparison of different H_2O_2 production in multiple runs with fresh medium. Filler medium: 750 μL, 350 mm^2 of particles*

5.6 Imaging techniques

First, microstructures were characterized by an optical microscope. The microstructures were pipetted onto a silicon/silicon dioxide wafer and imaged at different magnifications. Figure 29 shows that the particles make structures of multiple sizes. The gold and PN side is clearly distinguishable. For good photofaradaic behaviour, it is necessary to have both sides of the particle in contact with the medium. The larger particles were more likely to wrap up and group together. This effect is unwanted and we named it the ”burrito effect“. Therefore, one of the future objectives will be to develop techniques to produce more uniform particle formation.

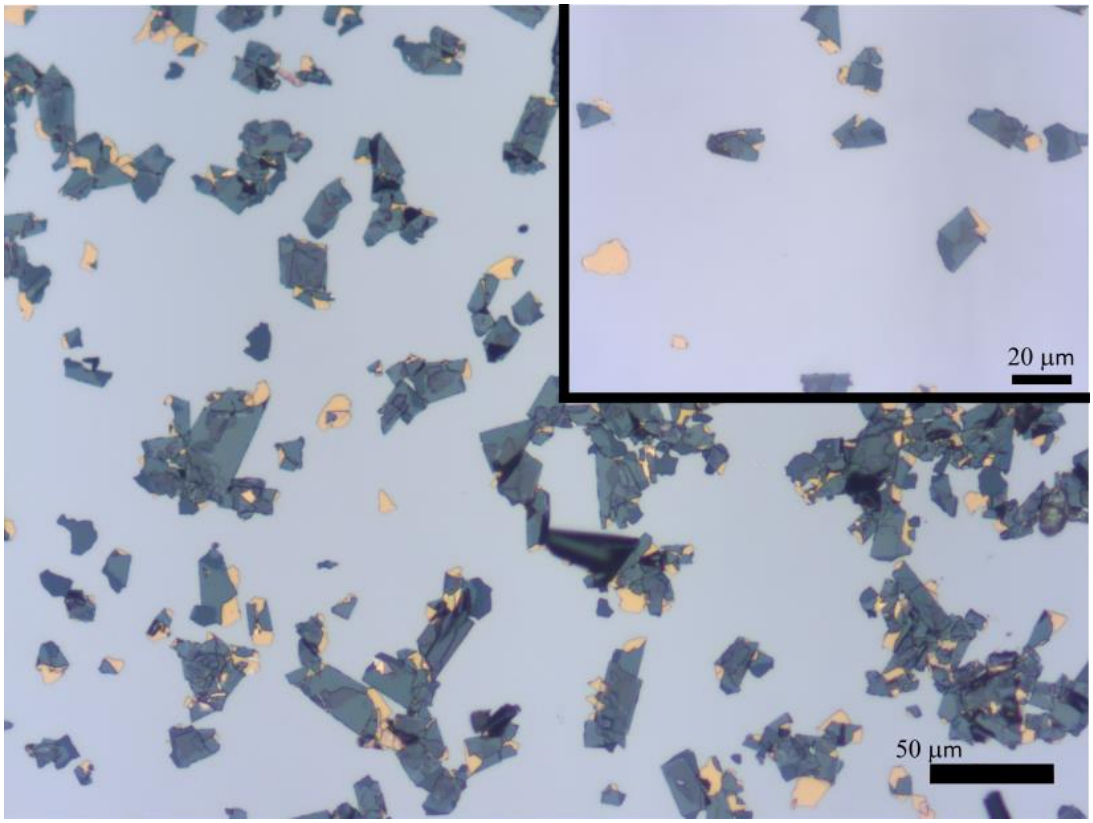

Figure 29 *Microparticles imaged using an optical light microscope.*

The particles were further investigated by a scanning electron microscope. For this purpose, the particles were dispensed directly on the SEM holder stub to provide good contact and reduce charging during imaging. Due to the organic character of the sample, the conditions of the electron beam must be adjusted. The acceleration voltage was set to 1 kV and the current to 6.3 pA. We used the integration of 1028 images with a fast scan rate (100 ns per line) to reduce the charging of the sample.

The border between the gold and PN layers is shown in Figure 30. The 15 nm Au layer (the smooth side) forms a great adhesion layer for the 60 nm of organic layer (nanocrystalline side). Where the particles crack seemed random, however in all cases the organic layer sticks well to the gold substrate.

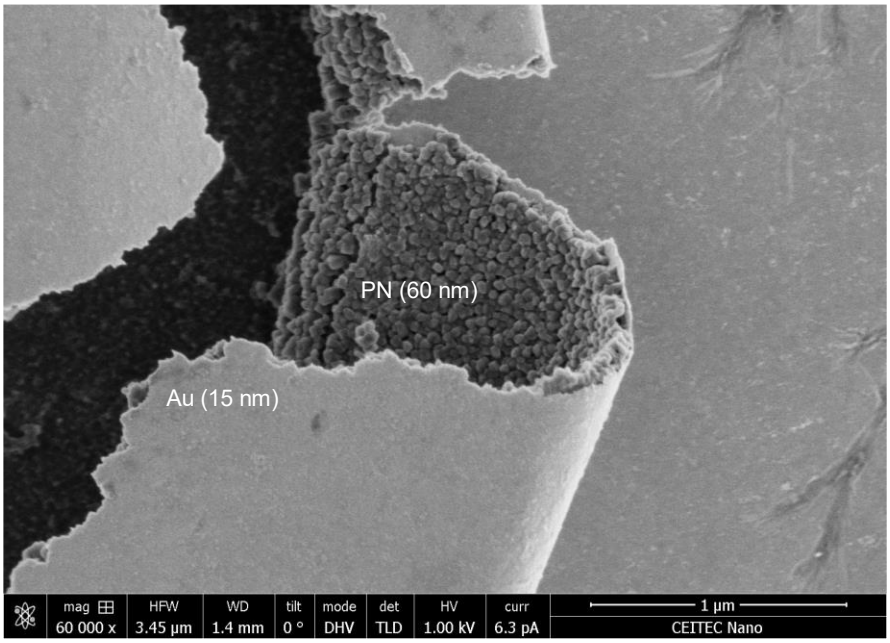

Figure 30 *Scanning electron microscopy image of the Au/PN interface.*

The ”burrito effect“ imaged by the electron microscope (Figure 31). The images provided with help of Radim Zahradníček (CEITEC Nano member). We assume that this phenomenon is caused by the compressive stress in the 15 nm gold. For future experiments, the thickness of the layer will be reduced and the effect will be further investigated.

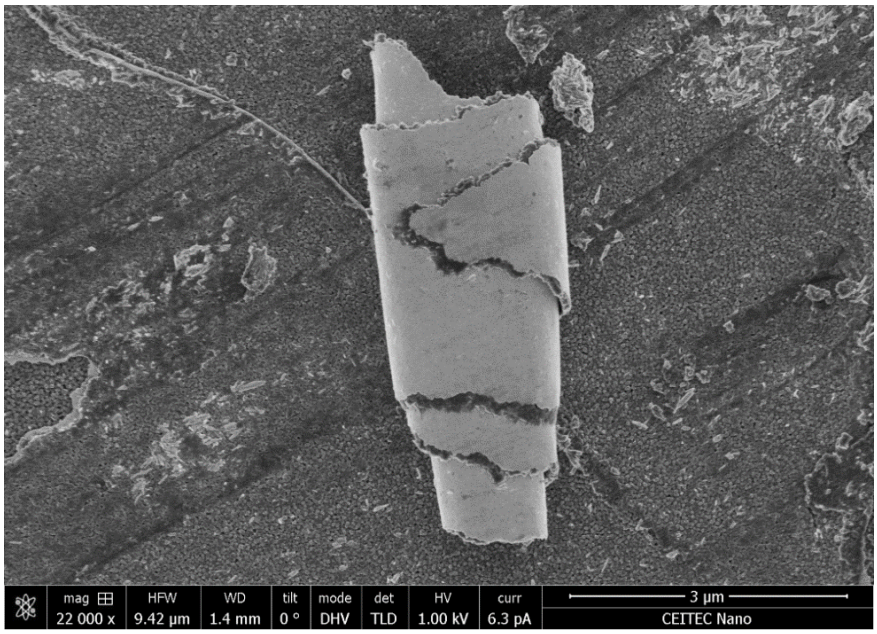

Figure 31 *Scanning electron microscopy image of the “burrito effect“.*

6 CONCLUSION

Semiconductor microstructures were fabricated using thin-film deposition techniques followed by delamination in an aqueous filler medium. Microstructures performed photofaradaic reactions resulting in the generation of reactive oxygen species. Hydrogen peroxide (H_2O_2) was produced by a two-electron oxygen reduction reaction with simultaneous oxidation of a sacrificial donor, of which sodium formate and HEPES proved the best. Particles were capable of sustained peroxide production by long-term exposure to deep red light. The redox reactions were proved for full stack devices (Au/PN) in comparison to bare layers, which were using the mechanism of autooxidation (PN) or plasmonic effects (Au). To mimic physiological conditions, the microparticle behavior was investigated in ACSF and PBS. According to the data, microstructures showed colloidal stability and the highest efficiency in ACSF, almost certainly due to the presence of the HEPES donor. It was proven that the choice of donor affects the final H_2O_2 production.

For future work, the microparticles can be tuned by coating them with co-catalysts. The additional layer should improve the catalytic activity of the gold layer. Next, the particles could be coated with surfactants to enhance the colloidal stability. The effect of ions in the medium should be investigated further especially concerning the different concentrations of ions. Additionally, the H_2O_2 production should be also examined for a light source with higher intensity, because there is a possibility to reach higher concentrations in a short period of time.

Controlled delivery of ROS is investigated as a possible route to cell stimulation. H_2O_2 acts as a signalling molecule and can be used to trigger an action potential. Since the microparticles developed herein could be injected onto a mature neural culture (Figure 32), without the need of culturing the cells on special substrates, they could be a great alternative for on-demand delivery of H_2O_2. We are planning exactly those experiments in collaboration with the Medical University of Graz.

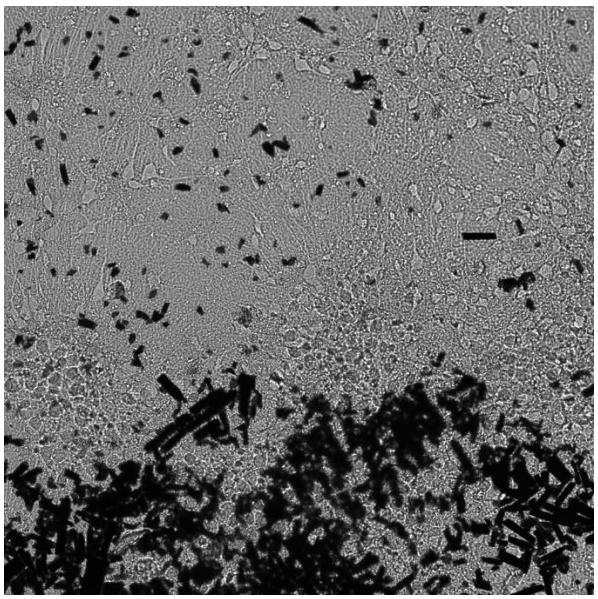

Figure 32 *Au/PN microparticles in tight contact with Cortical neurons of postnatal Sprague Dawley rats (P0-1) (Charles River).*
The image was provided by Tony Schmidt, MedUni Graz.

7 LITERATURE

[1] D. Rand *et al.*, 'Direct Electrical Neurostimulation with Organic Pigment Photocapacitors', *Advanced Materials*, vol. 30, no. 25, Jun. 2018, doi: 10.1002/adma.201707292.

[2] T. Schmidt *et al.*, 'Light Stimulation of Neurons on Organic Photocapacitors Induces Action Potentials with Millisecond Precision', *Adv Mater Technol*, vol. 7, no. 9, Sep. 2022, doi: 10.1002/admt.202101159.

[3] M. J. Donahue *et al.*, 'Wireless optoelectronic devices for vagus nerve stimulation in mice', *J Neural Eng*, vol. 19, no. 6, Dec. 2022, doi: 10.1088/1741-2552/aca1e3.

[4] M. Silverå Ejneby *et al.*, 'Chronic electrical stimulation of peripheral nerves via deep-red light transduced by an implanted organic photocapacitor', *Nat Biomed Eng*, vol. 6, no. 6, pp. 741–753, Jun. 2022, doi: 10.1038/s41551-021-00817-7.

[5] V. Đerek, D. Rand, L. Migliaccio, Y. Hanein, and E. D. Głowacki, 'Untangling Photofaradaic and Photocapacitive Effects in Organic Optoelectronic Stimulation Devices', *Front Bioeng Biotechnol*, vol. 8, Apr. 2020, doi: 10.3389/fbioe.2020.00284.

[6] M. Gryszel and E. D. Głowacki, 'Organic thin film photofaradaic pixels for on-demand electrochemistry in physiological conditions', *Chemical Communications*, vol. 56, no. 11, pp. 1705–1708, 2020, doi: 10.1039/c9cc09215c.

[7] H. Sies, 'Hydrogen peroxide as a central redox signaling molecule in physiological oxidative stress: Oxidative eustress', *Redox Biology*, vol. 11. Elsevier B.V., pp. 613–619, Apr. 01, 2017. doi: 10.1016/j.redox.2016.12.035.

[8] M. Zhang, Z. Tang, X. Liu, and J. Van der Spiegel, 'Electronic neural interfaces', *Nature Electronics*, vol. 3, no. 4. Nature Research, pp. 191–200, Apr. 01, 2020. doi: 10.1038/s41928-020-0390-3.

[9] S. Zhao, A. S. Mehta, and M. Zhao, 'Biomedical applications of electrical stimulation', *Cellular and Molecular Life Sciences*, vol. 77, no. 14. Springer, pp. 2681–2699, Jul. 01, 2020. doi: 10.1007/s00018-019-03446-1.

[10] A. Fasano, A. Daniele, and A. Albanese, 'Treatment of motor and non-motor features of Parkinson's disease with deep brain stimulation', *The Lancet Neurology*, vol. 11, no. 5. pp. 429–442, May 2012. doi: 10.1016/S1474-4422(12)70049-2.

[11] M. L. Kringelbach, N. Jenkinson, S. L. F. Owen, and T. Z. Aziz, 'Translational principles of deep brain stimulation', *Nature Reviews Neuroscience*, vol. 8, no. 8. pp. 623–635, Aug. 2007. doi: 10.1038/nrn2196.

[12] L. Bareket-Keren and Y. Hanein, 'Novel interfaces for light directed neuronal stimulation: Advances and challenges', *International Journal of Nanomedicine*, vol. 9, no. SUPPL.1. Dove Medical Press Ltd., pp. 65–83, May 06, 2014. doi: 10.2147/IJN.S51193.

[13] Gomer J. Charles, *Photodynamic Therapy: Methods and Protocols*. 2010. doi: 10.1007/978-1-60761-697-9.

[14] Mahmoudi Parisa, Veladi Hadi, and Pakdel G. Firooz, ‘Optogenetics, tools and applications in neurobiology’, *J Med Signals Sens*, vol. 7, no. 2, pp. 71–79, 2017.

[15] E. S. Albert *et al.*, ‘TRPV4 channels mediate the infrared laser-evoked response in sensory neurons’, *J Neurophysiol*, vol. 107, no. 12, pp. 3227–3234, Jun. 2012, doi: 10.1152/jn.00424.2011.

[16] F. Lodola, N. Martino, G. Tullii, G. Lanzani, and M. R. Antognazza, ‘Conjugated polymers mediate effective activation of the Mammalian Ion Channel Transient Receptor Potential Vanilloid 1’, *Sci Rep*, vol. 7, no. 1, Dec. 2017, doi: 10.1038/s41598-017-08541-6.

[17] M. Jakešová, ‘Wireless Bioelectronic Devices Driven by Deep Red Light’.

[18] N. S. Sariciftci, L. Smilowitz, A. J. Heeger, and F. Wudi, ‘Photoinduced Electron Transfer from a Conducting Polymer to Buckminsterfullerene’, *C. R. B. Lister, Geophys. J. R. Astron. Soc*, vol. 104, p. 8389, 1991, [Online]. Available: www.sciencemag.org

[19] M. Warczak, M. Gryszel, M. Jakešová, V. Derek, and E. D. Głowacki, ‘Organic semiconductor perylenetetracarboxylic diimide (PTCDI) electrodes for electrocatalytic reduction of oxygen to hydrogen peroxide’, *Chemical Communications*, vol. 54, no. 16, pp. 1960–1963, 2018, doi: 10.1039/c7cc08471d.

[20] E. Mitraka *et al.*, ‘Electrocatalytic Production of Hydrogen Peroxide with Poly(3,4-ethylenedioxythiophene) Electrodes’, *Adv Sustain Syst*, vol. 3, no. 2, 2019, doi: 10.1002/adsu.201800110.

[21] S. Günes, H. Neugebauer, and N. S. Sariciftci, ‘Conjugated polymer-based organic solar cells’, *Chem Rev*, vol. 107, no. 4, pp. 1324–1338, Apr. 2007, doi: 10.1021/cr050149z.

[22] J. Xue, ‘Perspectives on organic photovoltaics’, *Polymer Reviews*, vol. 50, no. 4, pp. 411–419, Oct. 2010, doi: 10.1080/15583724.2010.515766.

[23] M. Maniruzzaman, R. Abdur, M. A. Kuddus Sheikh, S. Singh, and J. Lee, ‘Conductive MoO3–PEDOT:PSS Composite Layer in MoO3/Au/MoO3–PEDOT:PSS Multilayer Electrode in ITO-Free Organic Solar Cells’, *Processes*, vol. 11, no. 2, Feb. 2023, doi: 10.3390/pr11020594.

[24] H. Hoppe and N. S. Sariciftci, ‘Organic solar cells: An overview’, *J Mater Res*, vol. 19, no. 7, pp. 1924–1945, Jul. 2004, doi: 10.1557/JMR.2004.0252.

[25] P. Peumans, A. Yakimov, and S. R. Forrest, ‘Small molecular weight organic thin-film photodetectors and solar cells’, *Journal of Applied Physics*, vol. 93, no. 7. pp. 3693–3723, Apr. 01, 2003. doi: 10.1063/1.1534621.

[26] W. Tang, ‘Two-layer organic photovoltaic cell c’, 1986. [Online]. Available: http://pubs.aip.org/aip/apl/article-pdf/48/2/183/7513936/183_1_online.pdf

[27] F. Missey, B. Botzanowski, L. Migliaccio, E. Acerbo, E. D. Głowacki, and A. Williamson, ‘Organic electrolytic photocapacitors for stimulation of the mouse somatosensory cortex’, doi: 10.1101/2021.10.20.465090.

[28] W. Geens, T. Aernouts, J. Poortmans, and G. Hadziioannou, ‘Organic co-evaporated films of a PPV-pentamer and C : model systems 60 for donoryacceptor polymer blends’, 2002.

[29] S. Günes, N. Marjanovic, J. M. Nedeljkovic, and N. S. Sariciftci, ‘Photovoltaic characterization of hybrid solar cells using surface modified TiO2 nanoparticles and poly(3-hexyl)thiophene’, *Nanotechnology*, vol. 19, no. 42, Oct. 2008, doi: 10.1088/0957-4484/19/42/424009.

[30] P. Schilinsky, C. Waldauf, and C. J. Brabec, ‘Performance analysis of printed bulk heterojunction solar cells’, *Adv Funct Mater*, vol. 16, no. 13, pp. 1669–1672, Sep. 2006, doi: 10.1002/adfm.200500581.

[31] S. E. Shaheen, R. Radspinner, N. Peyghambarian, and G. E. Jabbour, ‘Fabrication of bulk heterojunction plastic solar cells by screen printing’, *Appl Phys Lett*, vol. 79, no. 18, pp. 2996–2998, Oct. 2001, doi: 10.1063/1.1413501.

[32] D. T. Simon, E. O. Gabrielsson, K. Tybrandt, and M. Berggren, ‘Organic Bioelectronics: Bridging the Signaling Gap between Biology and Technology’, *Chemical Reviews*, vol. 116, no. 21. American Chemical Society, pp. 13009–13041, Nov. 09, 2016. doi: 10.1021/acs.chemrev.6b00146.

[33] R. Parameswaran and B. Tian, ‘Rational Design of Semiconductor Nanostructures for Functional Subcellular Interfaces’, *Acc Chem Res*, vol. 51, no. 5, pp. 1014–1022, May 2018, doi: 10.1021/acs.accounts.7b00555.

[34] M. Jakešová *et al.*, ‘Optoelectronic control of single cells using organic photocapacitors’, 2019.

[35] Maciej. Gryszel, *Organic electronic materials for hydrogen peroxide production*. Linköping University Electronic Press, 2020.

[36] M. Zangoli *et al.*, ‘Photoreactivity of Thiophene-Based Core@Shell Nanoparticles: The Effect of Photoinduced Charge Separation on In Vivo ROS Production’, *Journal of Physical Chemistry C*, vol. 127, no. 9, pp. 4672–4683, Mar. 2023, doi: 10.1021/acs.jpcc.2c06986.

[37] C. Bossio *et al.*, ‘Photocatalytic activity of polymer nanoparticles modulates intracellular calcium dynamics and reactive oxygen species in HEK-293 cells’, *Front Bioeng Biotechnol*, vol. 6, no. AUG, Aug. 2018, doi: 10.3389/fbioe.2018.00114.

[38] H. Sies and D. P. Jones, ‘Reactive oxygen species (ROS) as pleiotropic physiological signalling agents’, *Nature Reviews Molecular Cell Biology*, vol. 21, no. 7. Nature Research, pp. 363–383, Jul. 01, 2020. doi: 10.1038/s41580-020-0230-3.

[39] B. C. Dickinson, Y. Tang, Z. Chang, and C. J. Chang, ‘A nuclear-localized fluorescent hydrogen peroxide probe for monitoring sirtuin-mediated oxidative stress responses in vivo’, *Chem Biol*, vol. 18, no. 8, pp. 943–948, Aug. 2011, doi: 10.1016/j.chembiol.2011.07.005.

[40] G. Vilema-Enríquez, A. Arroyo, M. Grijalva, R. I. Amador-Zafra, and J. Camacho, ‘Molecular and cellular effects of hydrogen peroxide on human lung cancer

cells: Potential therapeutic implications', *Oxidative Medicine and Cellular Longevity*, vol. 2016. Hindawi Limited, 2016. doi: 10.1155/2016/1908164.

[41] K. Oka, B. Winther-Jensen, and H. Nishide, 'Organic π-Conjugated Polymers as Photocathode Materials for Visible-Light-Enhanced Hydrogen and Hydrogen Peroxide Production from Water', *Advanced Energy Materials*, vol. 11, no. 43. John Wiley and Sons Inc, Nov. 01, 2021. doi: 10.1002/aenm.202003724.

[42] D. A. Armstronga *et al.*, 'Standard electrode potentials involving radicals in aqueous solution: Inorganic radicals', *Bioinorg React Mech*, vol. 9, no. 1–4, pp. 59–61, Dec. 2013, doi: 10.1515/irm-2013-0005.

[43] I. Katsounaros *et al.*, 'Hydrogen peroxide electrochemistry on platinum: Towards understanding the oxygen reduction reaction mechanism', *Physical Chemistry Chemical Physics*, vol. 14, no. 20, pp. 7384–7391, May 2012, doi: 10.1039/c2cp40616k.

[44] J. Ehlich *et al.*, 'Direct measurement of oxygen reduction reactions at neurostimulation electrodes', *J Neural Eng*, vol. 19, no. 3, Jun. 2022, doi: 10.1088/1741-2552/ac77c0.

[45] A. Verdaguer-Casadevall *et al.*, 'Trends in the electrochemical synthesis of H2O2: Enhancing activity and selectivity by electrocatalytic site engineering', *Nano Lett*, vol. 14, no. 3, pp. 1603–1608, Mar. 2014, doi: 10.1021/nl500037x.

[46] X. Zhang *et al.*, 'Electrochemical oxygen reduction to hydrogen peroxide at practical rates in strong acidic media', *Nat Commun*, vol. 13, no. 1, Dec. 2022, doi: 10.1038/s41467-022-30337-0.

[47] S. Yang *et al.*, 'Toward the Decentralized Electrochemical Production of H2O2: A Focus on the Catalysis', *ACS Catalysis*, vol. 8, no. 5. American Chemical Society, pp. 4064–4081, May 04, 2018. doi: 10.1021/acscatal.8b00217.

[48] K. Mase, M. Yoneda, Y. Yamada, and S. Fukuzumi, 'Efficient Photocatalytic Production of Hydrogen Peroxide from Water and Dioxygen with Bismuth Vanadate and a Cobalt(II) Chlorin Complex', *ACS Energy Lett*, vol. 1, no. 5, pp. 913–919, Nov. 2016, doi: 10.1021/acsenergylett.6b00415.

[49] Byrne H. John and Riberts L. James, *From Molecules to Networks - An Introduction to Cellular and Molecular Neuroscience*. 2004.

[50] Y. Jiang *et al.*, 'Nongenetic optical neuromodulation with silicon-based materials', *Nat Protoc*, vol. 14, no. 5, pp. 1339–1376, May 2019, doi: 10.1038/s41596-019-0135-9.

[51] M. R. Antognazza, I. A. Aziz, and F. Lodola, 'Use of exogenous and endogenous photomediators as efficient ROS modulation tools: Results and perspectives for therapeutic purposes', *Oxidative Medicine and Cellular Longevity*, vol. 2019. Hindawi Limited, 2019. doi: 10.1155/2019/2867516.

[52] A. C.-H. Chen, Y.-Y. Huang, P. R. Arany, and M. R. Hamblin, 'Role of reactive oxygen species in low level light therapy', in *Mechanisms for Low-Light Therapy IV*, SPIE, Feb. 2009, p. 716502. doi: 10.1117/12.814890.

[53] J. T. Hancock', R. Desikan, and S. J. Neil1, 'Biochemical and Biomedical Aspects of Oxidative Modification Role of reactive oxygen species in cell signalling pathways', 2001.

[54] S. Gershman and A. Belkind, 'Plasma Cleaning of Surfaces', 2008, [Online]. Available: https://www.researchgate.net/publication/284486745

[55] N.-T. Nguyen, 'Fabrication technologies', in *Micromixers*, Elsevier, 2012, pp. 113–161. doi: 10.1016/b978-1-4377-3520-8.00004-8.

[56] K. A. Brown *et al.*, 'Light-driven dinitrogen reduction catalyzed by a CdS:nitrogenase MoFe protein biohybrid', *Science (1979)*, vol. 352, no. 6284, pp. 448–450, Apr. 2016, doi: 10.1126/science.aaf2091.

[57] V. Guerrero-Florez, S. C. Mendez-Sanchez, O. A. Patrón-Soberano, V. Rodríguez-González, D. Blach, and O. Fernando Martínez, 'Gold nanoparticle-mediated generation of reactive oxygen species during plasmonic photothermal therapy: A comparative study for different particle sizes, shapes, and surface conjugations', *J Mater Chem B*, vol. 8, no. 14, pp. 2862–2875, Apr. 2020, doi: 10.1039/d0tb00240b.

[58] A. Savva *et al.*, 'Photo-electrochemical stimulation of neurons with organic donor-acceptor heterojunctions', doi: 10.1101/2022.02.17.480608.

8 LIST OF ABBREVIATIONS

Abbreviation	Definition
ACSF	artificial cerebrospinal fluid
HRP	peroxidase from horseradish
H_2Pc	phthalocyanine
OEPC	organic electrolytic photocapacitor
OFET	organic field-effect transistor
OLED	organic light-emitting diode
OPV	organic photovoltaics
OTS	n-octyltriethoxysilane
PBS	phosphate buffer solution
PEDOT:PSS	poly(3,4-ethylene-dioxythiophene) polystyrene sulfonate
PVA	poly(vinyl)alcohol
PVD	physical vapor deposition
PVP	poly(vinyl)pyrrolidone
PSS	polystyrene sulfonate
PTCDI	Perylene tetracarboxylic diimide
QCM	quartz crystal microbalance
LED	light-emitting diode
ROS	reactive organic species
SEM	scanning electron microscopy
TMB	tetramethylbenzidine